universität wien

MASTERARBEIT / MASTER'S THESIS

Titel der Masterarbeit / Title of the Master's Thesis

Optimizing the Performance of the V0+ Detector of the Fast Interaction Trigger (FIT) for the ALICE Detector Upgrade

verfasst von / submitted by

Mohamed Awadein

angestrebter akademischer Grad / in partial fulfilment of the requirements for the degree of

Master of Science (MSc)

Wien, 2017 / Vienna, 2017

Studienkennzahl lt. Studienblatt / degree programme code as it appears on the student record sheet:	A 066 876
Studienrichtung lt. Studienblatt / degree programme as it appears on the student record sheet:	Masterstudium Physik
Betreut von /Supervisor:	Dr. Johann Zmeskal, Privatdoz.

Declaration of Authorship

I, Mohamed AWADEIN, declare that this thesis titled, "Optimizing The Performance of the V0+ Detector of the Fast Interaction Trigger (FIT) for the ALICE Detector Upgrade" and the work presented in it are my own. I confirm that:

- This work was done wholly while in candidature for the University of Vienna.
- Where any part of this thesis has previously been submitted for a degree or any other qualification at this University or any other institution, this has been clearly stated.
- Where I have consulted the published work of others, this is always clearly attributed.
- Where I have quoted from the work of others, the source is always given. With the exception of such quotations, this thesis is entirely my own work.
- I have acknowledged all main sources of help.
- Where the thesis is based on work done by myself jointly with others, I have made clear exactly what was done by others and what I have contributed myself.

Signed:

Date:

Abstract

"The ALICE Collaboration is preparing a major detector upgrade for the second LHC shutdown (2019-2020). The LHC luminosity and collision rate from 2021 onwards will exceed the parameters of the current ALICE forward trigger detectors. Moreover, the upcoming installation of a new Muon Forward Tracker will reduce the space for the upgraded trigger detector from one side. These conditions urge the need of a new design. The Fast Interaction Trigger (FIT) has been designed to replace the current ALICE forward trigger detector. The FIT will be the primary forward trigger and it will provide minimum bias trigger, multiplicity trigger, centrality, beam-gas event rejection, collision time for the Time of Flight detector (TOF), offline multiplicity and event plane determination" [1]. The FIT detector comprises of two subdetector systems, T0+ and V0+. The T0+ consists of two arrays of quartz radiators coupled to MCP-PMT sensors facing the interaction point. The V0+ detector is composed of a disk of plastic scintillator segments, optical fiber bundles, and photosensors. In this contribution, we will focus on the V0+ detector. The V0+ detector requires high efficiency, high dynamic range (1 - 500) particles, radiation hardness and must be compatible with 25 ns bunch spacing and $\sim$ 1-2 MHz interaction rate for pp collisions of the new LHC operation, while keeping the time resolution of about 200 ps for a single particle. In order to fulfill these technical challenges, a rigorous R&D work is ongoing. This thesis is focusing on optimization of scintillator material, the choice of photosensors (SiPM, Fine-mesh PMT, and MCP-PMT), the design of the optical fiber bundles and the readout electronics as well....

Zusammenfassung

Die ALICE-Kollaboration bereitet ein großes Detektor Upgrade für den zweiten LHC-Shutdown (2019-2020) vor. Die LHC-Luminosität und -Kollisionsrate wird ab 2021 die Design-Parameter des vorliegenden ALICE Detektors erheblich übersteigen. Darüber hinaus wird die Einführung eines neuen Myon Forward Trackers (MFT) das Platzangebot für die aktualisierten Trigger-Detektoren erheblich verringern. Zur Einhaltung dieser Bedingungen wurde ein Fast Interaction Trigger (FIT) entwickelt. Der FIT-Detektor besteht aus zwei Subdetektor-Systemen: T0+ und V0+. Der T0+ Detektor besteht aus zwei Anordnungen von Quarz-Radiatoren mit MCP-PMT-Sensoren, die auf den Interaktionspunkt gerichtet sind. Der V0+ Detektor besteht aus Kunststoff Szintillator Scheibensegmenten, Glasfaser-Bündel und Photosensoren. In dieser Arbeit konzentrieren wir uns auf den V0+ Detektor. Der V0+ Detektor erfordert hohe Effizienz, hohen Dynamikbereich (1-500) Partikel, Strahlunghärte und muss kompatibel sein mit einem 25 ns Abstand der Teilchenschauer und 1-2 MHz Interaktionsrate für pp-Kollisionen im neuen LHC-Betrieb; unter Beibehaltung der zeitlichen Auflösung von etwa 200 ps für ein einzelnes Teilchen. Um diesen technischen Herausforderungen gerecht zu werden, ist eine strikte fortlaufende F&E Arbeit erforderlich. Diese Arbeit konzentriert sich auf Optimierung des Szintillator Materials, die Wahl der Photosensoren (SiPM, Finemesh PMT und MCP-PMT), die Gestaltung der Glasfaser-Bündel, sowie die Ausleseelektronik.. . .

Acknowledgements

I would like to express my gratitude to Dr. Johann Zmeskal, Dr. Eberhard Widmann, Dr. Ken Suzuki and Dr. Michael Weber of the Stefan Meyer Institute for subatomic physics for the useful comments, remarks, and engagement through the learning process of this master thesis. Furthermore, I would also like to thank the experts who were involved in my laboratory work Dr. Lukas Gruber, and Dr. Gamal Ahmed for introducing me to the topic as well for the support on the way during my laboratory work. Also, I like to thank the participants from the ALICE collaboration, Dr. V. Grabski, Dr. A.Menchaca, and Dr. R. Alfaro of the Instituto de Fisica Universidad Nacional Autonoma de Mexico who have willingly shared their experience and their efforts during the beam times in CERN. I would like to thank my loved ones, who have supported me throughout the entire process, both by keeping me harmonious and helping me. I will be grateful forever for your assist. Special thank for the university of Vienna and the Austrian academy of science.. . .

Mohamed Awadein

Contents

List of Figures

List of Tables

List of Abbreviations

FIT	**F**ast **I**nteractions **T**rigger
ALICE	**A** **L**arge **C**ollider **E**xperiment
LHC	**L**arge **H**adron **C**ollider
IP	**I**nteraction **P**oint
QCD	**Q**uantum **C**hromo**d**ynamics
MIP	**M**inimum **I**onizing **P**article
p.e.	**p**hoto **e**lectron
MPV	**M**ost **P**robable **V**alue
SiPM	**Si**licon **P**hoto**m**ultipliers
NA	**N**umerical **A**perture
LED	**L**ight **E**mitting **D**iodee
LS2	**L**ong **S**hutdowng **2**
FOT	**F**iber **O**tical **T**aper
QE	**Q**uantum **E**fficiency
CE	**C**ollection **E**fficiency
TTS	**T**ransit **T**ime **S**pread
SMI	**S**tefan **M**eyr **I**nstitute
AC	**A**lternative **C**urrent
DC	**D**irect **C**urrent
FWHM	**F**ull **W**idth **H**alf **M**aximum
NIM	**N**uclear **I**nstrumentation **M**odule

To my father, Elsayed Awadein, who passed away in 2014. Although he is no longer physically presents in my life, I still feel his impact every day, To my great mother Zeinab, my wonderful wife, my amazing brothers Ahmed and Mahmoud, for their ongoing love, assist, providing me with unfailing support and continuous encouragement, and to all of my family and friends, Without whom none of my success would be possible. . .

Chapter 1

The Fast Interaction Trigger Upgrade for ALICE

1.1 Introduction

"ALICE at the Large Hadron Collider (LHC) is different in purpose and design of the other experiments at the LHC. Its main objective is the study of head-on collisions between heavy nuclei, mainly lead-lead at the highest achieved energy of the LHC. In these reactions, the LHC's tremendous energy–collisions of Pb nuclei produce energy 100 times more than those of the protons, the achieved temperature of such collision is 100,000 times higher than the temperature in the sun's core" cited from [2]. "Nucleons melt down into their elementary constituents to form for instant the fundamental matters which filled the universe until a few microseconds after the the Big Bang, the universe was filled with all kinds of particles expanding at almost the speed of the light. This mixture was dominated by quarks and gluons, such collision gives precise insights into the state of the universe a few millionths of a second after the Big Bang. The ALICE detector has to measure most of the produced particles, summing up to tremendous number of produced particles in each of these 'little bangs', and recording their number, type, mass, energy and direction, in order to deduce from the produced debris the existence and the properties of matter under these conditions produced by the collision" cited from [3]. "ALICE consists of several detector systems for measuring hadrons, leptons, and photons. It is designed to perform measurements of high-energy nucleus-nucleus collision in order to study quark matter (QCD matter) under a high temperature and density. During the Quark Matter 2012 conference, it was announced that ALICE experiment produced Quark-Gluon Plasma (QGP) with a temperature of about 5.5 trillion degrees. The data has been successfully analyzed from proton-proton, lead-lead, and proton-lead collisions during the past years till now" cited from [4].

1.2 ALICE Detector Overview

"ALICE detector refers to a small detector, but for ALICE we mean relatively 'small' in the context of LHC: The detector is 16 m height, 16 m wide and 26 m long and weighs about 10,000 tons. The detector consists of 17 complex sub-detectors, each has a certain function and design constraints to perform a specific task and provide a certain information about the detected particle" cited from [2]. "A sketch drawing of ALICE is shown in Figure (1.1). It comprises a central part, which is able to measure photons, electrons, and hadrons, a forward single arm spectrometer is used for muon detection. The central 'barrel' part covers the direction vertical to the beam from 45° to 135° and is placed inside a very large solenoid magnet, As a warm resistive magnet, the maximum field at the nominal power of 4 MW reaches 0.5 T. The central barrel contains many tracking detectors, that record the momentum of the charged particles by determining the curvature of their paths when they move inside the magnetic field" cited from [3] [5]. "These particles will be identified and sorted out in terms of their masses and types using a series of particle identification detectors, followed by two different types of electromagnetic calorimeters for measuring jets and photons. The forward muon arm (2°-9°) consists of a complex arrangement of absorbers, a large dipole magnet, and fourteen planes of tracking and triggering chambers" cited from [3].

1.3 ALICE Detector Upgrade

"With a view to getting a maximum benefit of the high potential of the LHC upgrade performed during the Long Shutdown 2 (LS2), the ALICE collaboration takes over the upgrade of the detector performance in order to comply with the new conditions of the LHC-operation. The development and the improvement of the ALICE detector will enable a quantitative characterization of the high density and high-temperature phase of strongly interacting matter, und trying to observe new phenomena in QCD. With the proposed timeline of initiating a high-rate operation after the 2018 LS2, the objectives of the upgrade plans will be achieved by collecting data into the 2020s decades. The study of the strongly interacting state of matter following LS2 will focus on rare probes and the study of their coupling with the medium and hadronization processes. These include heavy-flavour mesons and baryons, quarkonium states, low-mass dieleptons, jets and their correlations with other probes. To achieve the goals described above, high statistics and high precision measurements are needed" cited from [1].

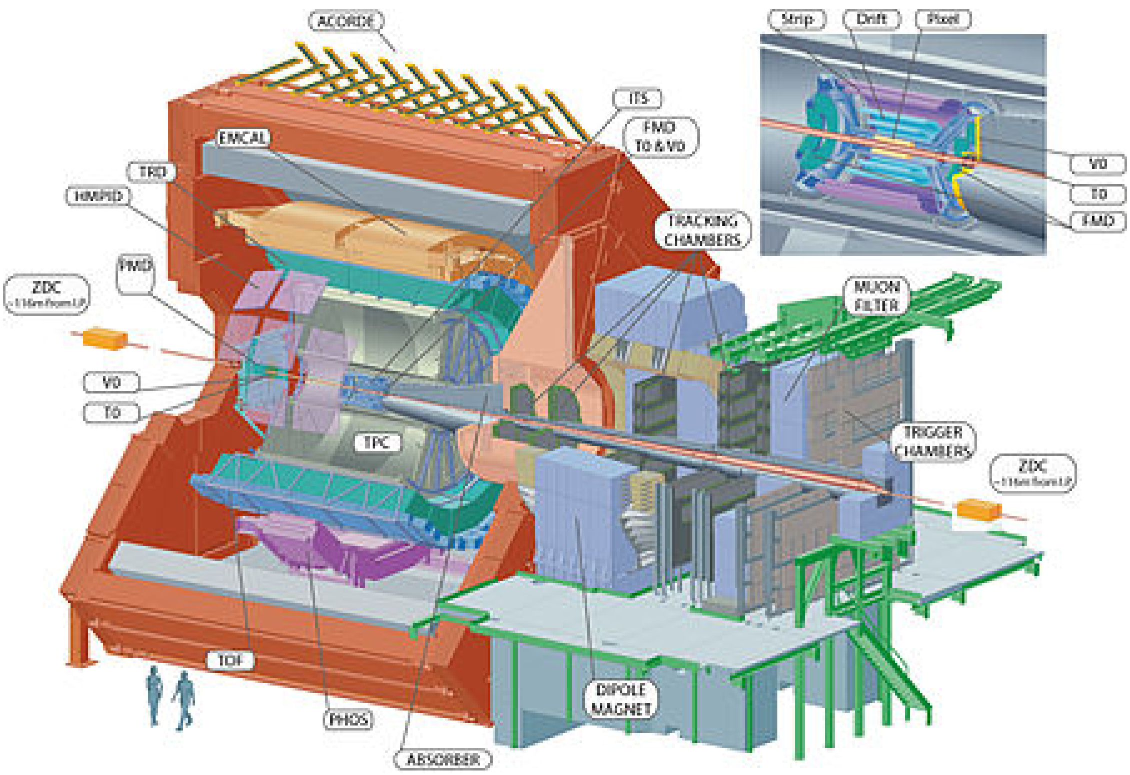

FIGURE 1.1: Summary and schematics of the ALICE detector upgrade [2].

"Many of these measurements will involve some complex probes at low transverse momentum, where traditional methods for triggering will not be applicable anymore. Therefore, the ALICE collaboration is going to upgrade the current detector by improving its low-momentum vertexing and tracking capability and allowing data taking at extensively higher rates. The upgrade strategy is based on the expectation that the luminosity[1] of the LHC will be extremely increased after the 2nd shutdown with lead beams reaching an interaction rate of 50 kHz or instantaneous luminosities of $L = 6 \times 10^{27} cm^{-2} s^{-1}$. In the proposed upgrade, the ALICE detector will be modified such that all the interactions will be inspected [1]. The upgrades plan will preserve the current particle identification capability while improving the vertex detector, triggering and tracking capabilities. The main parts of the ALICE detector are shown in Figure (1.1), more detail will be found at [7], [8],[9], [10]" cited from [1].

1.4 The Fast Interaction Trigger (FIT)

"The ALICE trigger upgrade master plan is based on having at least 10 nb^{-1} of Pb-Pb collisions at luminosities $\sim$ to $L = 6 \times 10^{27} cm^{-2} s^{-1}$ at collision rates of 50 kHz, where each collision is sent to the online systems, either by a Minimum Bias trigger or by a self-trigger" cited from [1].

"In order to achieve that, the Fast Interaction Trigger [11] has been proposed to discriminate beam-beam interactions with 99 % efficiency to provide a start signal for the rest of the ALICE detector (Level 0 trigger) with a time resolution (σ) $\sim$ 30 ps. For the evaluation and rejection of beam- induced background, in particular, beam-gas interactions the FIT detector will find the vertex location with a performance of at least 40 ps time resolution and 50% vertex efficiency for p-p collisions, and 21 ps time resolution and close to 100% vertex efficiency for Pb-Pb central and semi-central collisions. Eventually, the FIT detector is expected to be able to measure the reaction event plane with a resolution of 80% at around 20% centrality, 40% resolution for central collisions and 10%

[1] It is a measurement of how many collisions can be produced in a detector per cm^2 and per second. To calculate the number of collisions cross section has to be considered [6].

resolution for the most peripheral Pb-Pb collisions. Finally, the FIT detectors will give a feed-back to the LHC for luminosity monitoring" cited from [1].

"The current ALICE detector has two forward detector systems, including the T0 [12], and the V0 [13] that provides a minimum bias trigger, multiplicity trigger, beam-gas event rejection, collision time for time of flight (TOF), online multiplicity and event plane (EP) determination. In order to comply these functionalities to the collision rates of the ALICE upgrade, it is important and crucial to finding a new solution with the Fast Interaction Trigger. The best way to approaching the upgrade requirements for the FIT is increasing the acceptance of the current T0. However, using the current setup of the T0 for the T0-Plus detector of a quartz + Photomultiplier tube (PMT) is not possible anymore as it is hard to fit the space allocated to the trigger detector after the installation of the Muon Forward Tracker. Instead, a new concept of an array of modules consists of segmented quartz radiators attached directly to a microchannel plate-PMT (MCP-PMT) is suggested" cited from [1]. A preliminary design of the upgrade for the trigger detectors is shown in Figure (1.2) and Figure (1.3).

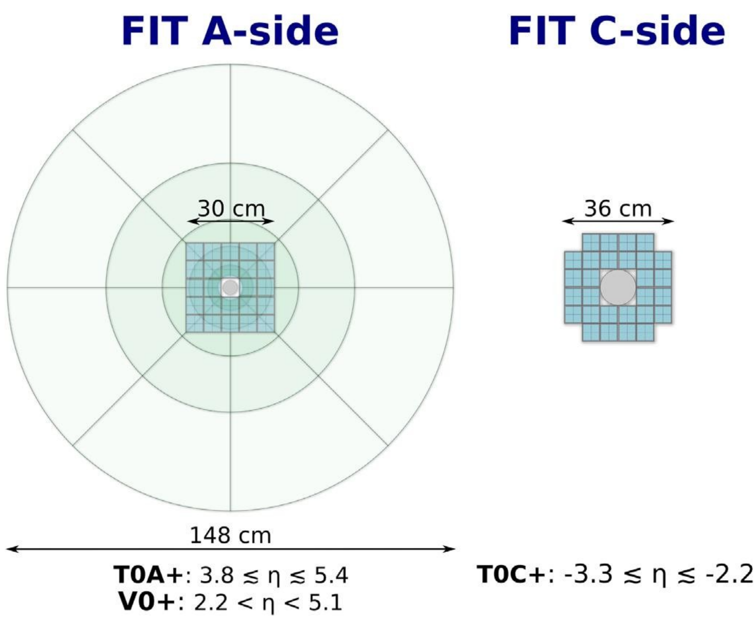

FIGURE 1.2: Scaled drawings of FIT components on both sides of the IP. The opening in the middle of the T0+ array on the C-side is needed to provide clearance for an R = 60 mm flange on the beam pipe cited from [1].

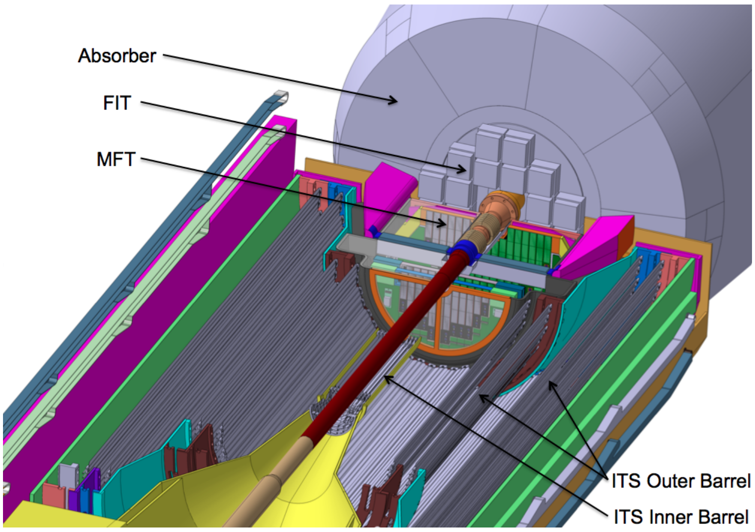

FIGURE 1.3: Detectors on the C-side cited from [1].

1.4.1 The FIT Detectors T0+ and V0+

"Each T0+ module consists of a 2 cm thick quartz radiators attached to a developed Planacon XP85012 MCP-PMT. The size of the radiators fits that of the photocathode with an active area covers about 80 % of the front surface of the sensor. The granularity of the sensors was increased in order to improve its performance at high particle multiplicities. The anode of the Planacon consists of 64 sectors which operate independently. So that the Cherenkov radiators can be subdivided to minimize optical crosstalk. Also, by subdividing the radiator into small sections, one increases the light loss due to the reflections from the inner walls" cited from [1]. "The best performance of T0+ modules was achieved by arranging the anodes and dividing the radiator into 4 sectors. During the prototype tests with 6 GeV/c pions and electrons from CERN PS, the 4-sector T0+ modules reach time resolution of 25 ps (σ). The active part of the V0+ detector will be a 4 cm thick ring made of EJ-204 plastic scintillator with an inner diameter of 8 cm and an outer diameter of 148 cm. The detector will be divided into five concentric rings and eight 45-degree sectors for a total of 40 elements. The light collection from the scintillators will be collected by 1 mm diameter optical fibers, assembled on a two-dimensional matrix with 5 mm pitch. The matrix is coupled directly to the scintillator while on the other side, the fibers are bundled and, via a trapezoid light guide coupled to light sensors or directly coupled to the photosensor" cited from[1]. "The main influence of the V0+ scintillator ring is to improve the centrality and reaction plane resolution as well as adding sensitivity for the beam-gas events detection. As compared to the current V0 detector, V0+ will have 3.2 times larger active area, 25 % more readout channels, and a better time resolution. By the use of high developed micro-PMTs, SiPM and/or with MCP-PMT sensors, V0+ is expected to decrease the aging problems and the after-pulses that observed in the current V0 detector. During beam times, the prototypes were tested with 6 GeV/c pions and electrons from CERN PS, the V0+ modules showed a time resolution of 210 ps (1 σ) and 35 % amplitude resolution (FWHM), uniform across the area of the scintillator, when using Fine mesh PMTs" cited from [1].

Chapter 2

V0+ Detector Prototype

2.1 Introduction

The geometry and segmentation of V0+ will closely resemble that of the V0 detector. A ring made of plastic scintillators will be located at the distance of around 3.3 m from the IP Figure (1.2). It corresponds to the pseudorapidity range $2.2 < \eta < 5.1$. The scintillator will be divided into four concentric rings. Each ring will be further subdivided into 8 equal 45° slices. Unfortunately, the available space on the C-side excludes the possibility of installing a scintillator detector there in addition to the 20 T0+ modules, so it will be installed only at the A-side. The main improvements of the V0+ detector as compared to its predecessor are improving light collection scheme, new light sensor, radiation hardening, electronics, readout and significantly reduced fiber length between the scintillator and the light sensor [14]. In this chapter, I will discuss the design of the V0+ detector prototype and give an overview of the data analysis of the beam time in October 2015.

2.2 The Principle of the V0+ Design

The prototype was mainly designed by the Mexican group of (Instituto de Fisica Universidad Nacional Autonoma de Mexico), it has 3 main and one optional part.

The main parts :

- Scintilator.

- Fibers.

- Optical sensor.

The optional part :

- Light concentrator.

Each part of the detector will be explained in detail in (Chapter 3). The first part is a scintillator that used to produce light whenever a charged particle passes through it, this light is collected by a matrix of fibers, these fibers are fixed on a plexiglass plate from one side, this plexiglass plate is fixed on the top of the box that holds the scintillator to connect the fibers to the scintillator. The other terminal of the optical fibers is bundled and coupled to a photosensor to convert the produced light into an electrical signal, see Figure (2.1) and Figure (2.2). Optical grease was placed between the fibers and the scintillator and between the fibers and the photosensor, see Figure (2.3).

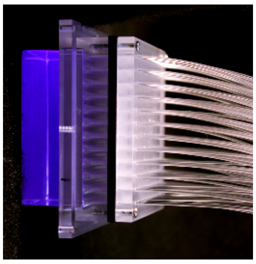

FIGURE 2.1: Light collection scheme of V0+ detector (Photograph by W.H.Trzaska)

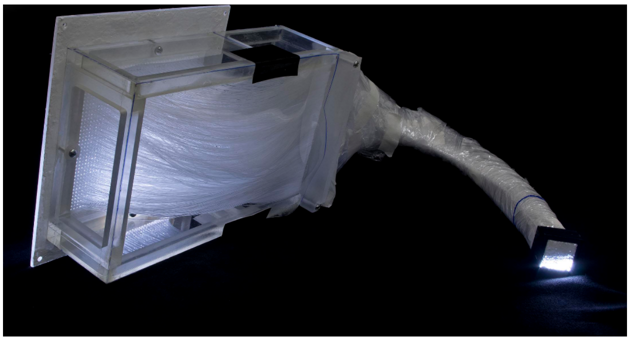

FIGURE 2.2: Fiber bundle of V0+ detector. (Photograph by W.H.Trzaska)

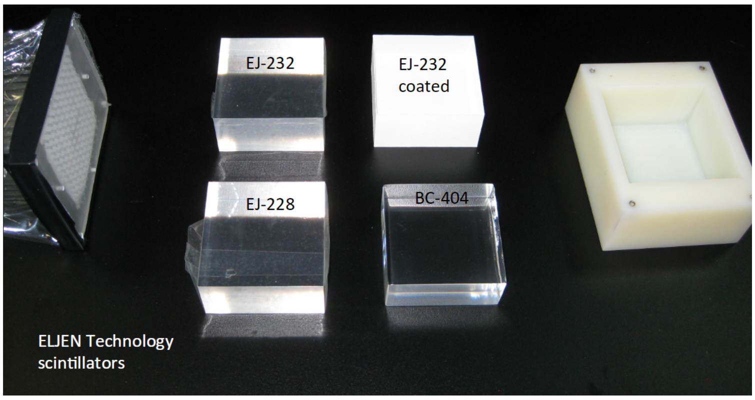

FIGURE 2.3: Different scintillator materials and a box to hold the scintillator to connect it with fibers (Photograph by W.H.Trzaska).

2.3 Review of the Beam Time in October 2015

Different types of photosensors, fiber bundles and different materials of the scintillator were tested during this beam time to determine the best performance. This beam time gave us a first date set. In this chapter, we will focus on the results of the fiber bundles made of Kuraray fibers with silicon photomultiplier (SiPM), see Figure (2.4), as we were looking forward to build and design a new prototype with only one SiPM readout.

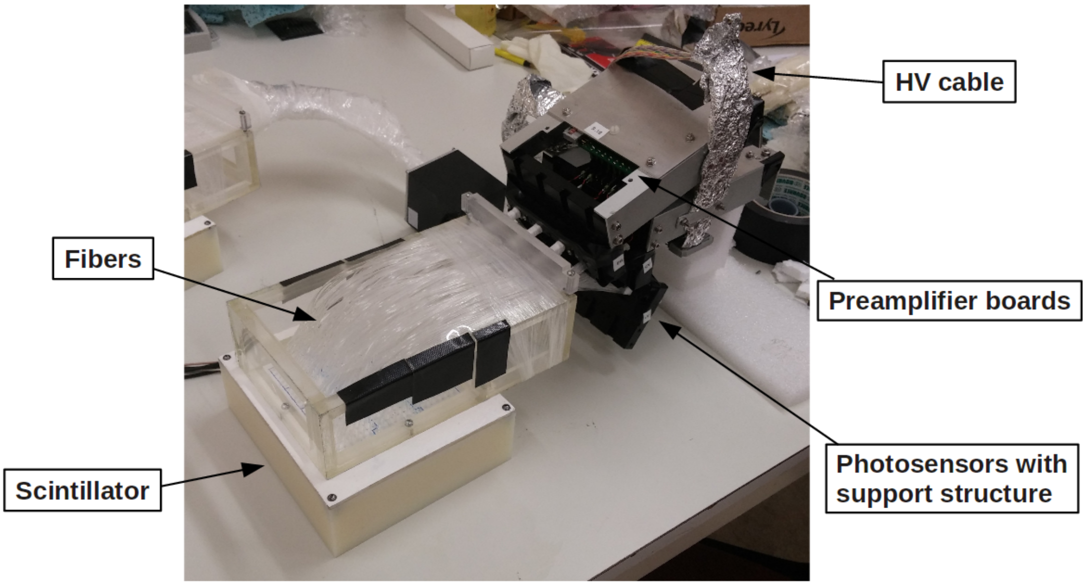

FIGURE 2.4: 400 Kuraray multi-clad clear fibers form 10x10cm^2 matrix, Length: 25 cm, 1 mm diameter, 5 mm pitch, 12 bundles (Photograph by V. Grabski).

2.3.1 Experimental Setup

The measurements were carried out in the East hall at CERN using T10 of PS facility [1] beam (mainly produces a beam of pions and electrons), see Figure (2.5). The data taking started from Oct 8 till Oct 18, in total more than 40 different runs (conditions). Two different fiber bundles were tested, one fiber bundles in combination with 12 SiPM photosensor readout, and the second one was designed to be coupled to either PMT or MCP-PMT. Both of the fiber bundles were tested in combination with different scintillator material with size of 10x10x4 cm^3. The 2 prototypes were laid back to back in a dark closed box to prevent any amount of light to infiltrate inside the box and might affect the actual read of the SiPM, see Figure (2.6).

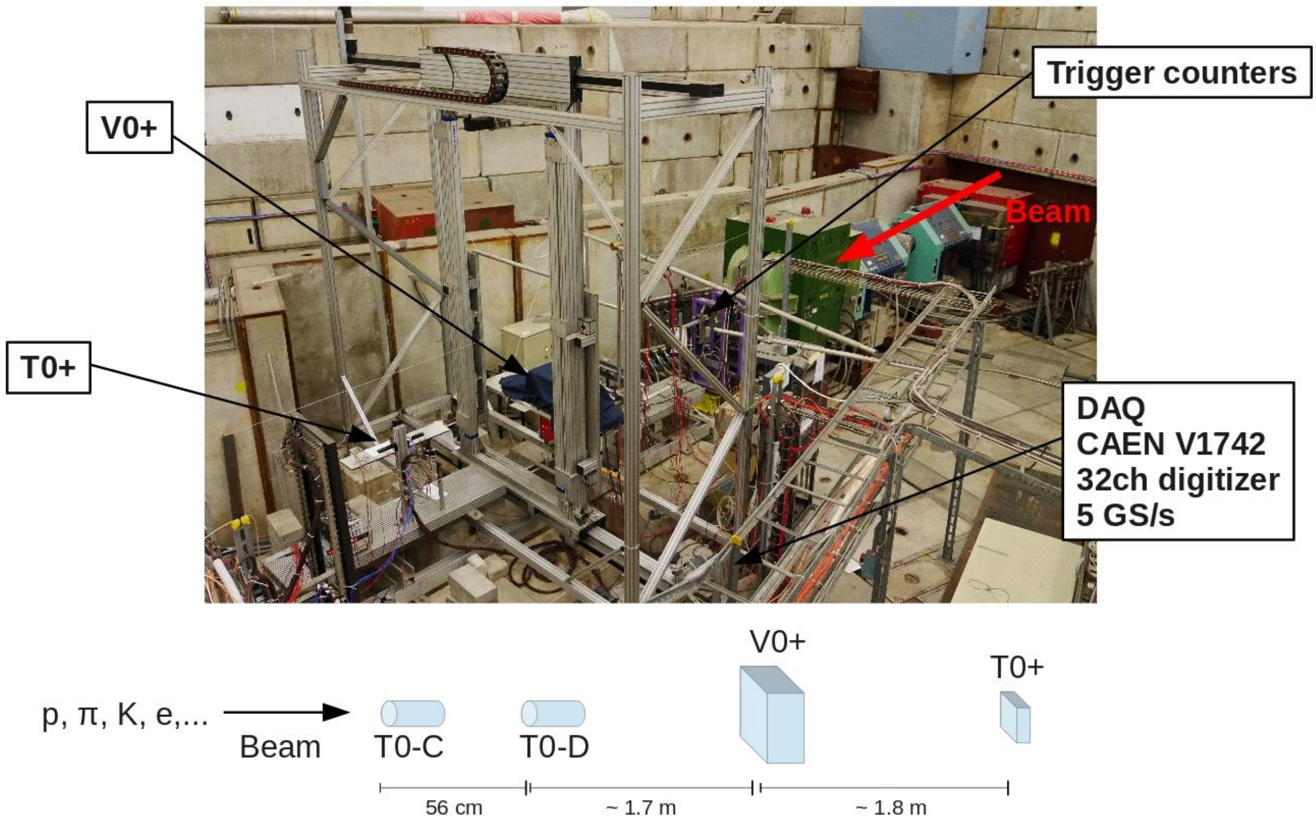

FIGURE 2.5: The position of the detectors in T10. (Photograph by W.H.Trzaska)

The V0+ detector was placed downstream from the Cherenkov telescope, composed of 4 quartz radiator coupled to PLANACON XP85012 MCP-PMT. The T0-C and T0-D are

[1]The T10 beam is a secondary beam that delivers secondary particles up to 7 GeV/c at a production angle of 61.6 milliradians [15].

PMTs each coupled to a scintillator, the coincidence signal from T0-C, T0-D, and T0+ was the trigger for V0+.

FIGURE 2.6: The box with 2 detectors placed next to each other to be tested in one run. (Photograph by W.H.Trzaska)

Components of the V0+ prototype SiPM

As it was mentioned before that we will focus only on the prototype configuration with SiPM photosensor. Only the results and the data analysis of this prototype will be shown in detail [16], see Figure (2.4).

The Scintillator: 100 x 100 x 40 mm^3.

- Material: Plastic Eljen scintillators EJ-232, EJ-228.
- Surface: White paint, Teflon, Aluminium foil.

The Fibers: 400 Kuraray multi-clad clear fiber formed in 10 x 10 cm^2 matrix, arranged in 12 bundles with 25 cm Length, diameter ϕ 1 mm and 5 mm Pitch Figure (2.4).

Photosensors: Ketek SiPMs 6x6 mm^2 with 10k pixels Figure (2.7).

Electronics: "Self-made" preamplifier adapter boards, Photonique AMP-0604 preamplifier with gain $\sim$ 20.

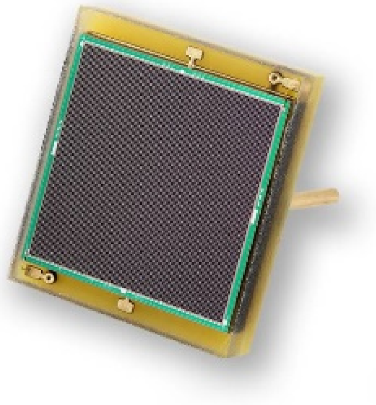

FIGURE 2.7: Photosensor Ketek 6x6 mm^2[17].

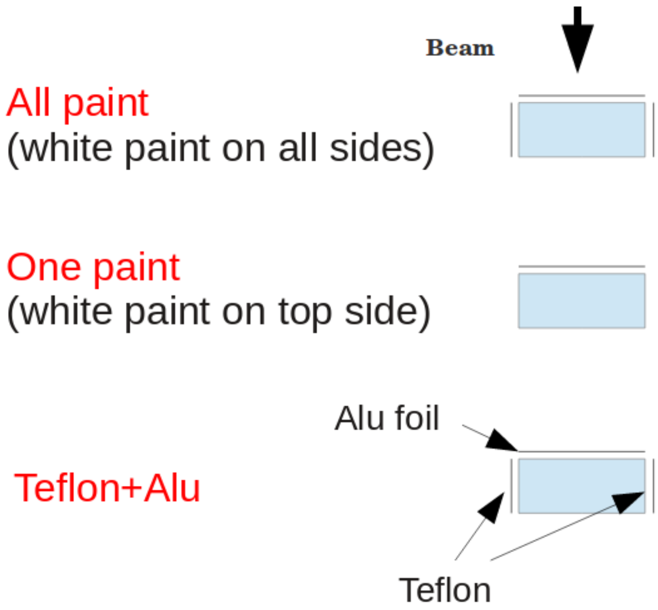

FIGURE 2.8: The different coating and wrapping of Scintillator Materials (L.Gurber).

2.4 Results and Data Analysis of October 2015 Beam Time

2.4.1 Results of Scintillator Materials

The Scintillators were tested with different paints and wrapping to determine which one gives a better time resolution and gain, see Figure (2.8).

Time Resolution: The best result was achieved with EJ-228 one side painted. Time resolution $\sigma = 231.4 \pm 1.2$ ps at a bias voltage of 30 V, see Figure (2.9).

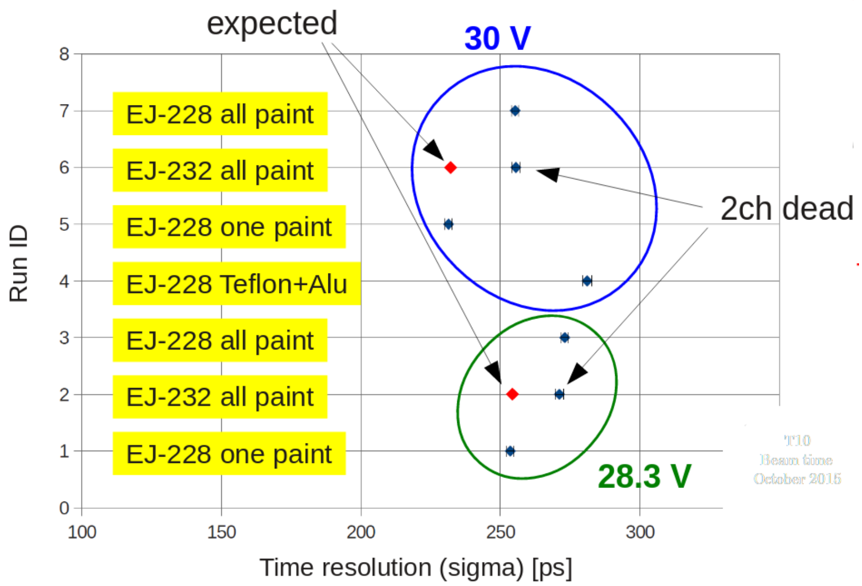

FIGURE 2.9: Comparison between time resolution of different Scintillators in different surface paints and coating. During the measurements, some channels were dead, the red points stands for the expected results if all the channels were working and the blue points are the actual values (L.Gurber).

Figure (2.10) shows the position dependency of time resolution.

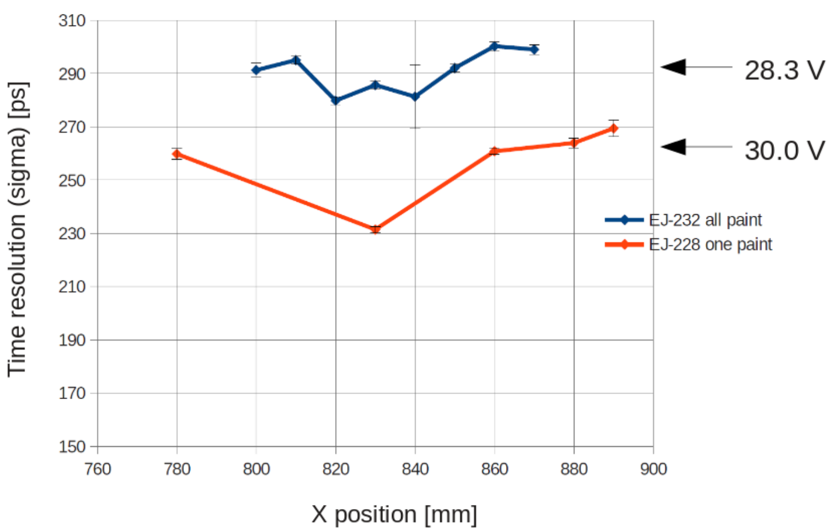

FIGURE 2.10: Time resolution dependency of position. The x-position has the arbitrary scale with a range of the scintillator's width (100 mm) (L.Gurber).

The pules height of this prototype detector shows a position dependency as well, see Figure (2.11).

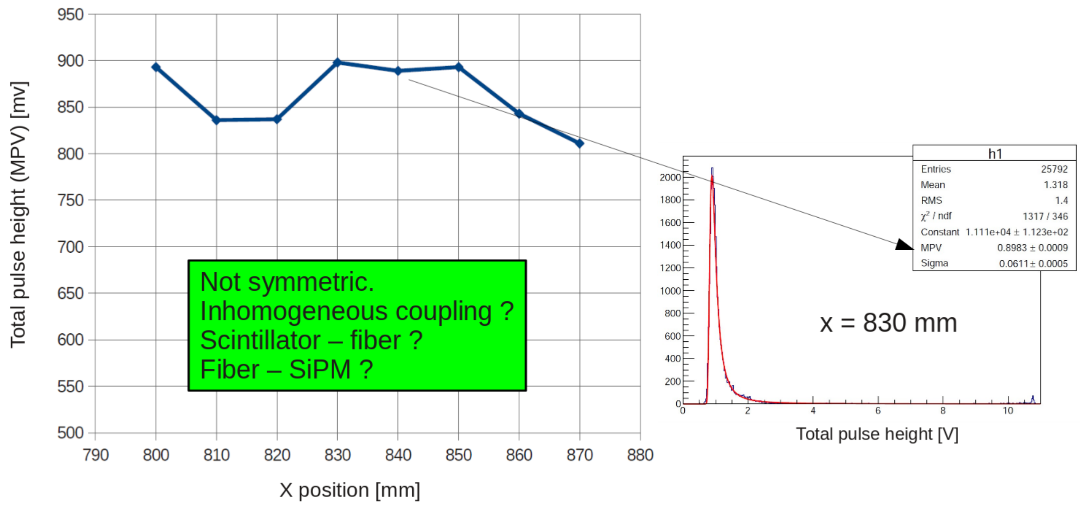

FIGURE 2.11: position dependency on pulse amplitude. this could be either due to inhomogeneous coupling between scintillator-fiber or fiber-SiPM. (L.Gurber)

2.4.2 Test of Light Guides and Lenses

During the Oct2015 beam time we also tested some light guides “Winston cone”[2] produced by Edmund optics with additional optical lenses, in order to reduce the number of fibers, see (2.12).

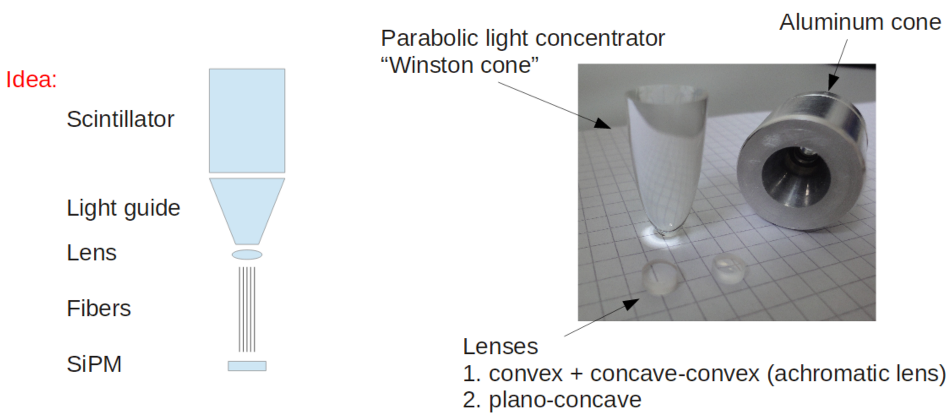

FIGURE 2.12: Winston cone and lenses used to reduce the number of fibers (L.Gurber).

[2] "A Winston cone is a light collector in the shape of an off-axis parabola of revolution with a reflective inner surface. It concentrates the light passing through a relatively large entrance aperture through a smaller exit aperture. The collection of incoming rays is maximized by allowing off-axis rays to make multiple reflections before reaching the exit aperture. Winston cones are used to concentrate light from a large area onto a smaller photodetector or photomultiplier. They are widely used for measurements in the far-infrared region of the electromagnetic spectrum, in part, because there are no suitable materials to form lenses in that range. Winston cones take their name from their inventor, the physicist Roland Winston" cited from [18].

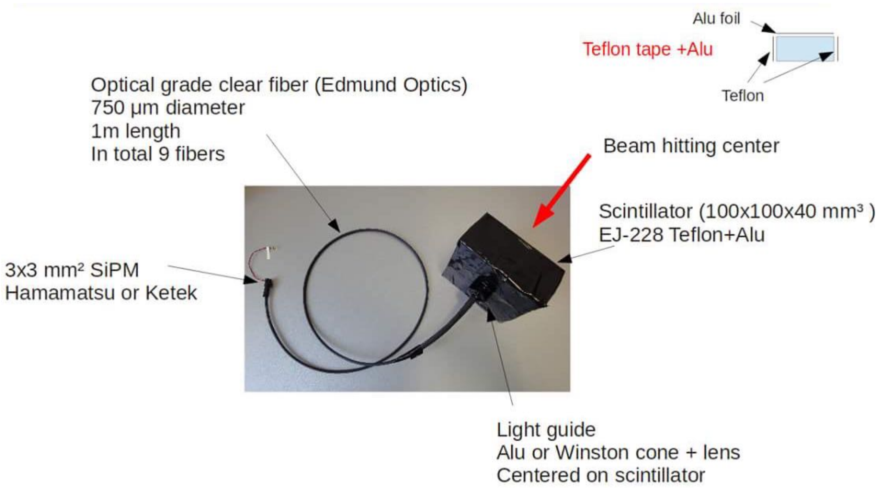

FIGURE 2.13: The detector with Winston cone (L.Gurber).

Signal Rise Time

The signal of the SiPM (SiPM voltage set to 28.3 V $\sim$ 10% over-voltage) gives a rise time of 15-20 ns. The SiPM signal has to distinguish between 2 signals within a time interval 25 ns, as the bunch crossing of the LHC will be 25 ns. The faster the output signal the more efficient to be used at a high frequency.

Chapter 3

Contribution of the V0+ Prototype Detector with SiPM Photosensor

3.1 Introduction

In this chapter, design and build of a new prototype (SMI prototype) to optimize the V0+ performance will be explained in detail. A new prototype of the V0+ detector was designed based on the Mexican prototypes. It has only one SiPM readout photosensor instead of 12 SiPMs as in the old design and an optional light concentrator to reduce the number of fibers. The new design aims to improve the time resolution, position independence, higher dynamic range[1], low cost, and radiation hardening by using fiber and place the SiPM photosensor a bit far from the IP. The prototype has four parts, see Figure (3.1).

1. Scintillator.
2. Primary optical fiber bundle, and Secondary optical fiber bundle (optional).
3. Light concentrator (optional).
4. Photosensor.

The new design of the fiber bundle enables to use a single SiPM photosensor by using an optional fiber bundle and a light concentrator. PMT or MCP-PMT could be used as well with this design by attaching the primary fiber directly to them. Figure (3.2) shows

[1]The detector's dynamic range. In general, a detector fulfills the condition of linearity

the fiber configuration of the prototype setup. In configuration A, only PMT and MCP-PMT photosensor can be used due to the bundle size. However, SiPM could be used in B and C configuration.

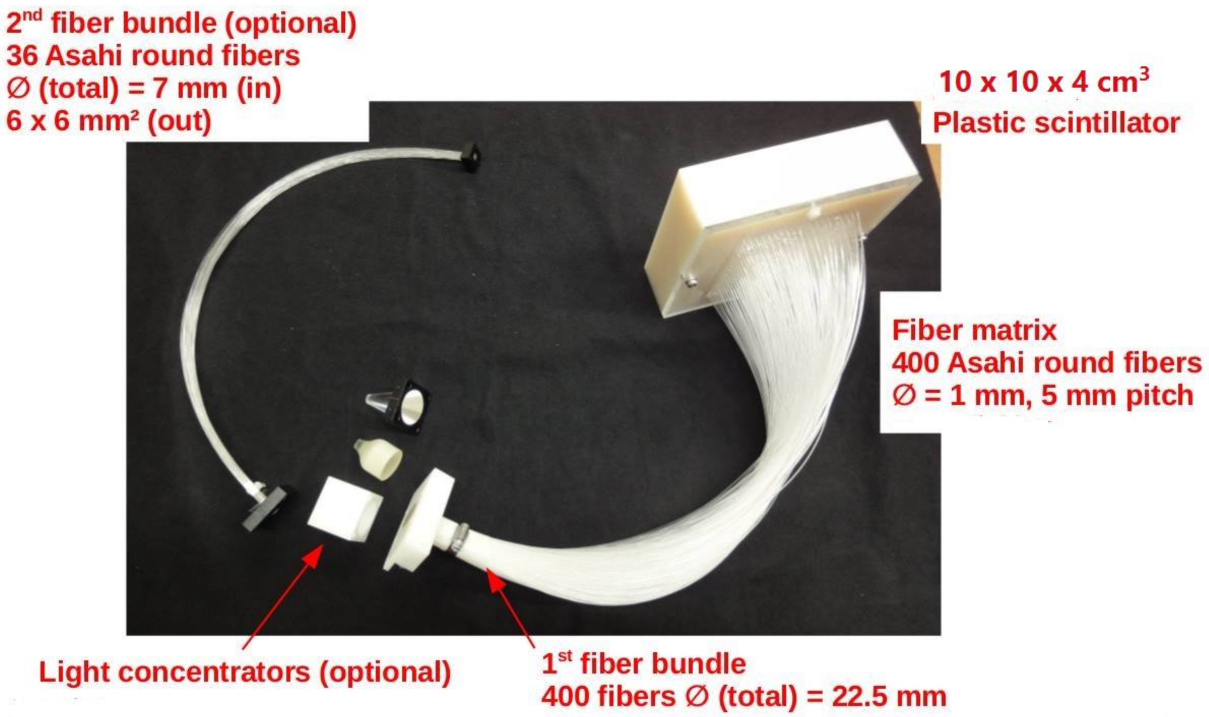

FIGURE 3.1: V0+ prototype built in SMI (Photograph by W.H.Trzaska).

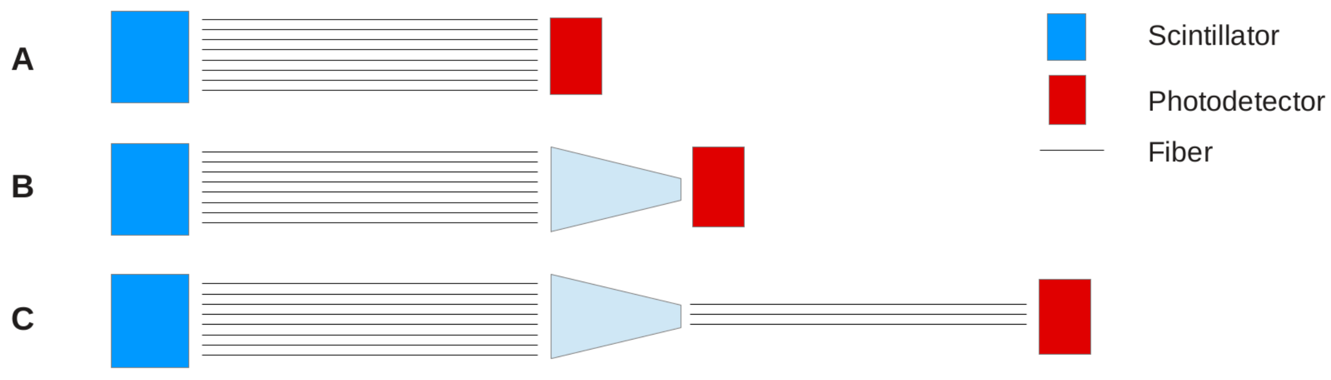

FIGURE 3.2: Fiber configuration for the prototype setup with and without light concnetrator.

3.2 Scintillators

The tested scintillators for our detector prototype were organic as it needs a very fast signal. Two 10x10x4 cm^3 scintillators (produced by Eljen technology) were tested during the beam times in 2016:

EJ-204: "has the highest scintillation efficiency of any of Eljen's plastic scintillators, along with the combination of high speed and good attenuation length. It is suited for high-performance detector systems for nuclear and high-energy physics research. Its emission wavelength is near 400 nm" cited from [19].

EJ-228: "should be used in small sizes for the best timing results, with the largest scintillator dimension less than 10 cm to minimize photon scattering effects. This scintillator is useful where very high count rates are present" cited from [19].

3.3 Design and Preparation of the Fiber Bundle of the SMI Prototype

Fibers are used to collect the light from the scintillator by using a matrix of 20 x 20 fibers distributed over 10 x 10 cm^2. Fibers are important as well to protect the photosensor from radiation, so the photosensor could be placed a bit far from interaction point IP. The used fiber for this prototype is Asahi fiber with a diameter of ϕ 1 mm.

Fiber cut 400 fibers were cut precisely to a length of 50 cm and other 36 fibers with a length of 60 cm using a sharp cut machine. Every single fiber was aligned over a scaled board and they have been cut one by one.

Fibers polishing was done in several stages:

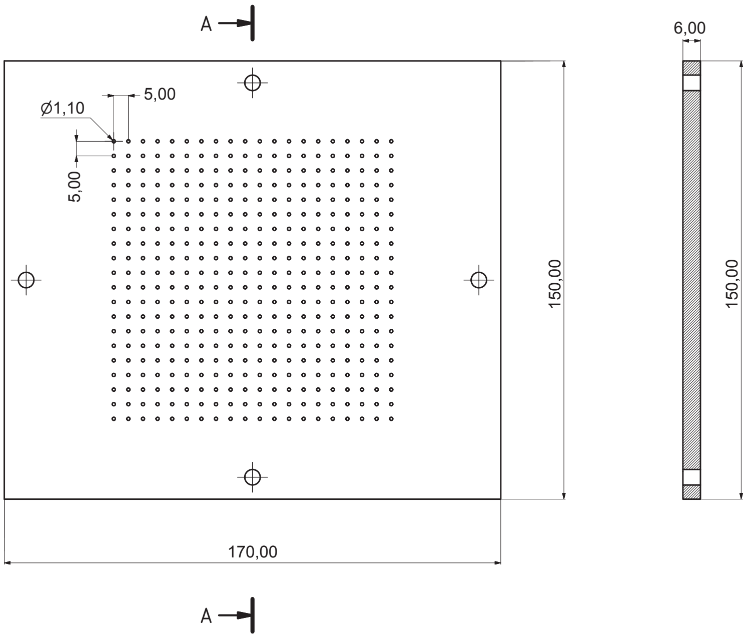

FIGURE 3.3: Sketch of the plexiglas cover (designed by Doris Pristauz-Telsnigg).

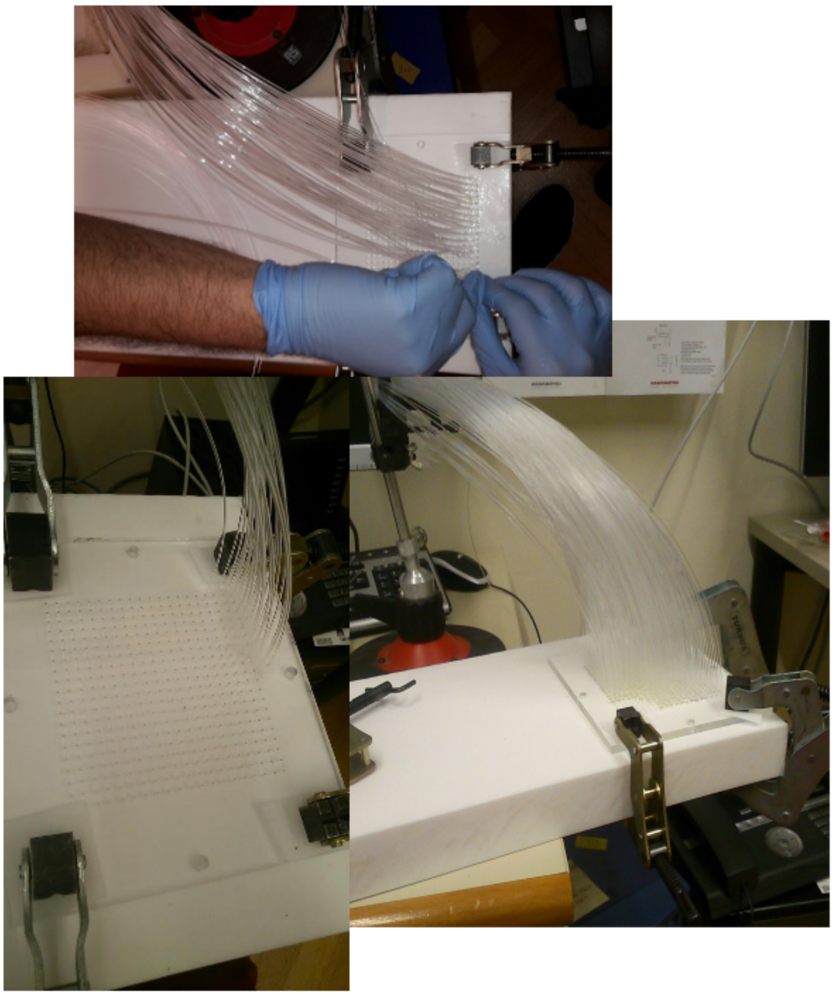

FIGURE 3.4: Preparing the optical fibers in plexiglass plate using glue.

The cut fibers were stuck inside a cover made out of plexiglass (this cover connects the scintillator to the fibers and it has 400 slots) by adding glue to the tip of every single fiber from on end, see Figure (3.3). The plexiglass plate was fixed over a teflon sheet to make sure that the fibers were aligned to the surface as shown in Figure (3.4), then we left it for 24 hours till the glue got hard to be ready for polishing. Before starting the polishing, the plate was tested using an optical lens to check if all the fibers were fixed to the top of the plate surface, the defected fibers were adjusted to the correct position, see Figure (3.5). The glued fibers in the plate were polished by moving the sandpaper in a circular motion under running water using different types of sandpaper starting with rougher to smoother one.

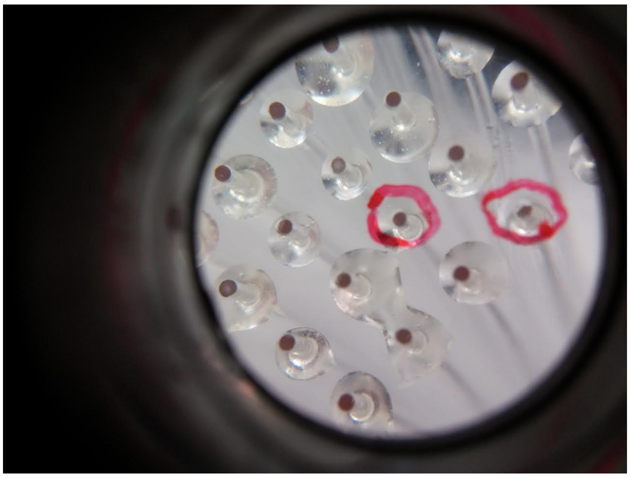

FIGURE 3.5: Picture was taken using magnifying glass to check every single fiber on the plate and correct the flaws.

The other end of the fibers was bundled in one round bundle, their surface was aligned, then optical glue was added. The capillary action[2] enabled the glue to move between the fibers up to almost 5 cm, so that the fiber cladding has not been damaged during the polishing, Figure (3.6). In the same way as before, these fibers were polished in a circular motion under running water using different sandpaper starting with rougher to smoother one, Figure (3.7).

[2]Capillary action is the ability of a liquid to flow in narrow spaces without the assistance of, or even in opposition to, external forces like gravity.

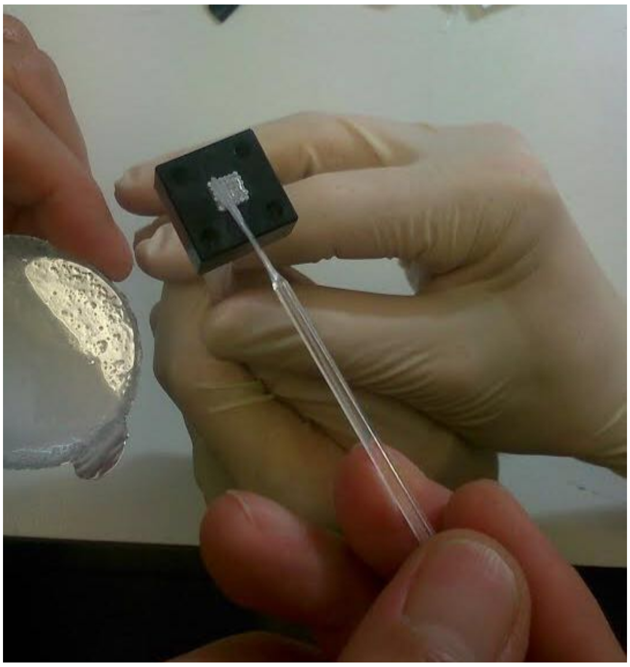

FIGURE 3.6: Adding the optical glue to the fiber bundle.

FIGURE 3.7: Polishing under running water.

3.4 Light Concentrator

The main purpose of using the light concentrator is to reduce the number of fibers to use only one SiPM and increase the dynamic range. Two types of the light concentrators were tested to estimate the light transmission efficiency and the efficiency dependence on the position. Two types of light concentrators were tested:

1. **Fiber Optical Taper (FOT):** The FOT was produced by OJSC «Plant «Optic». Its

small end has a diameter ϕ of 9 mm, the big end has a diameter ϕ of 30 mm [20]. See Figure (3.8).

2. **Plastic Light Guide:** An alternative plastic light guide made out of acrylic glass fabricated at SMI workshop, with a diameter ϕ of 9 mm of the small end, the big end has a diameter ϕ of 30 mm, see Figure (3.9).

FIGURE 3.8: Fiber Optical Taper (FOT).

FIGURE 3.9: A plastic light guide made out of acrylic glass with holder.

Several tests were performed to understand the behavior of light transmission of the FOT and the plastic light guide in order to know if it could improve the performance of V0+ detector.

3.4.1 Measuring the Total Efficiency of Light Transmission

Experimental setup consists of **two rubber masks** one has an aperture with diameter of 30 mm and the other has an aperture with diameter of 9 mm; **LED** with a light exit angle of 16^o; **Photomultiplier tube (PMT)** Phillips XP2020 (applied bias voltage 1900 V); **Light diffuser** with an angle of 20^o. The experimental setup is shown in Figure (3.10).

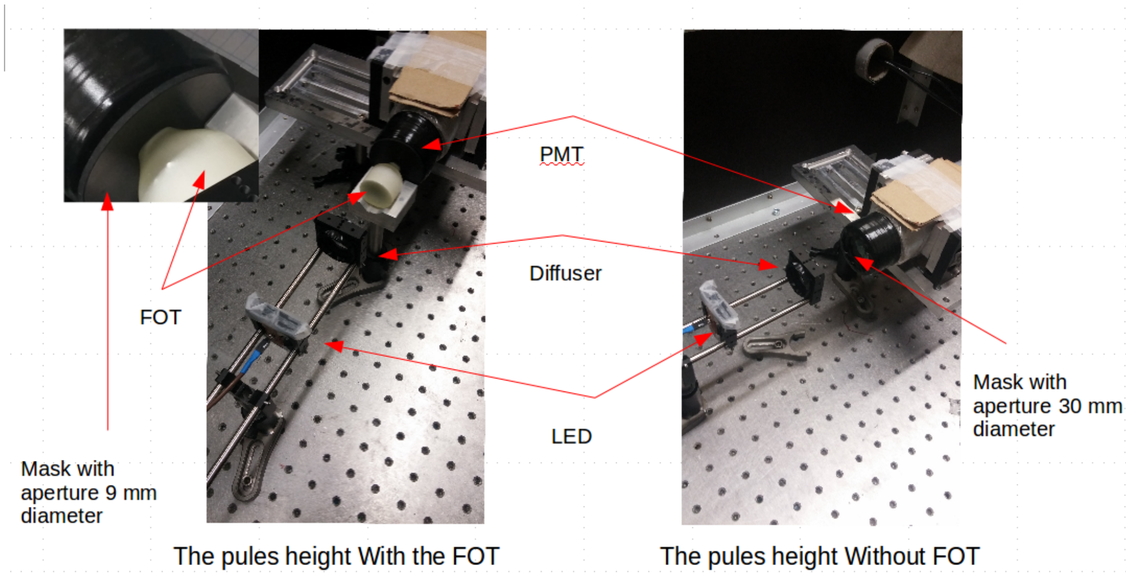

FIGURE 3.10: The setup of the FOT total efficiency measurement.

The mask with aperture of 30 mm diameter (the same area of the big base of the FOT) was placed to cover the window of the PMT, in order to expose it to the same amount of light as for the big base of the FOT. The distance between the LED and the light diffuser = 8 cm. The distance between the light diffuser and the PM = 6 cm. The LED was triggered with a NIM pulse with 1 kHz frequency.

The total efficiency of light transmission is the ratio between the amplitude of PMT's signal, when the FOT is connected to the PMT to the amplitude of PMT's signal without FOT, under the exposure to the same light intensity.

The reference value or the signal amplitude without the FOT was determined to be (3.44 ± 0.002) V, Figure (3.11).

The next step is to measure the amount of light passing through the FOT when the same amount of light fell on its big base as before, as shown on the left side of Figure

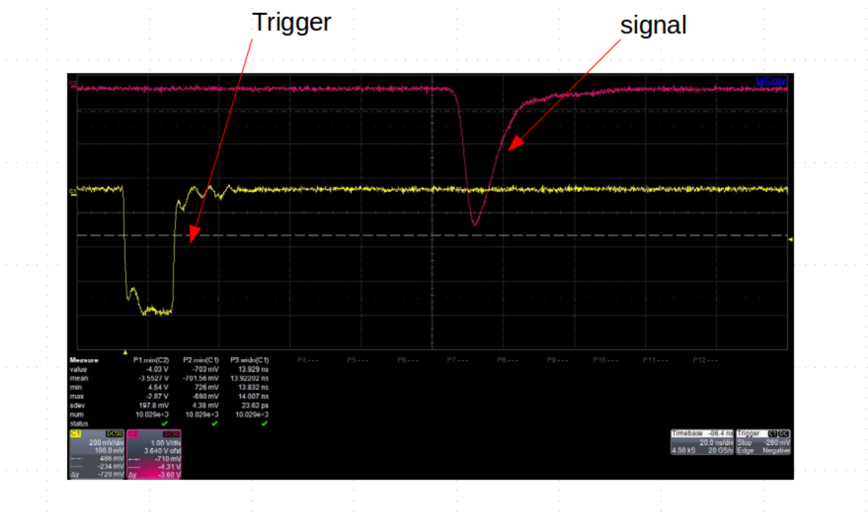

FIGURE 3.11: A screen-shot from the oscilloscope shows the pulse height without FOT.

(3.10). The PMT window was covered with a mask with ϕ 9 mm to enable only the light came from the small base of the FOT to be detected. Then the FOT was placed to stuck to the PMT, optical grease was added between the FOT and PMT surface. The distance between the LED and the Diffuser = 8 cm and the distance between the big base of the FOT and the diffuser = 6cm The obtained pulse height was 1.4 $\pm$ 0.001 V. **The total transmission efficiency** ϵ = 41$\pm$4 %. This measurement shows the average efficiency of the FOT.

3.4.2 Scanning the Position Efficiency of the FOT

This test was performed to measure the efficiency at different points on the FOT and emulating more actual conditions similar to the coupling configuration between the FOT and the fiber bundles as in option C in Figure (3.2). **Experimental setup** is made of a single fiber with diameter of 0.75 mm coupled to the LED, a plastic mask with diameter ϕ of 30 mm with 15 apertures across each diameter in x-axis and y-axis, the distance between two adjacent apertures is 2 mm and the distance between the mask edge to the first aperture is 0.5 mm. The applied bias voltage of the PMT is -1785 V Figure (3.12).

The light coming from the fiber was directly coupled to the PMT (without the FOT),

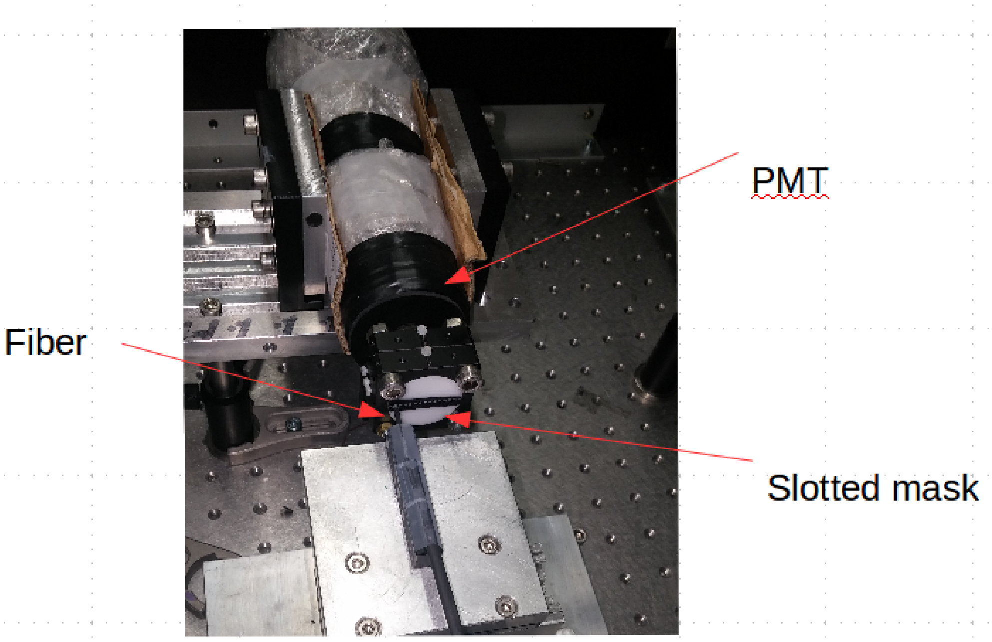

FIGURE 3.12: Scanning the position efficiency of the FOT using optical fiber.

the measured reference value was = 7.08 V. after that, the small base of the FOT was coupled into the PMT, while the plastic mask was fixed on the big base of the FOT, the signal height was measured at 15 positions across the x-axis and y-axis, by sticking the fiber in each aperture. Optical grease was added before sticking the fiber inside every single aperture, the value of the pulse height was divided by the reference value to calculate the efficiency at each point. Table (A.1) and Table (A.2) show the values of the efficiency at each point on the FOT. The average efficiency was calculated by integrating the efficiency across x-axis and y-axis analytically Figure (3.13).

The Average efficiency from the integration ϵ = 31±4 %. The integration was done assuming that each point at the same distance from the center has the same efficiency ϵ. To demonstrate how the integration was done, see Figure (3.14), the small black points represent the points where the efficiency was measured, the circle was divided into discs, each disc has 4 points (except at the center of the circle) locate at the same distance from the center, the average of this 4 values was calculated per each sector then multiplied by the quotient of the disc area to the total area. Adding up all the sectors gives the average efficiency over the whole area. Equation (3.1) can be applied to determine the average efficiency.

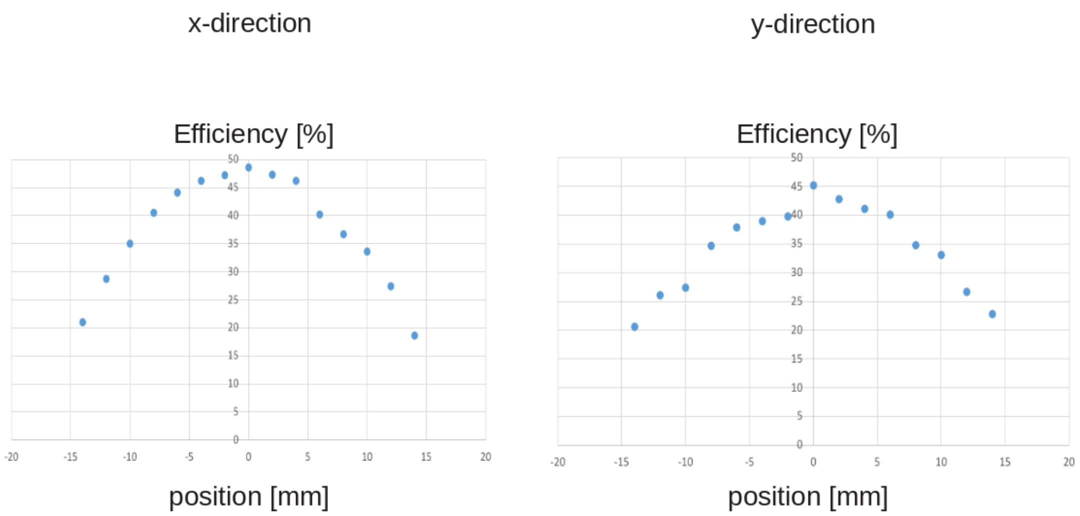

FIGURE 3.13: The efficiency of the position scan in x-axis and y-axis.

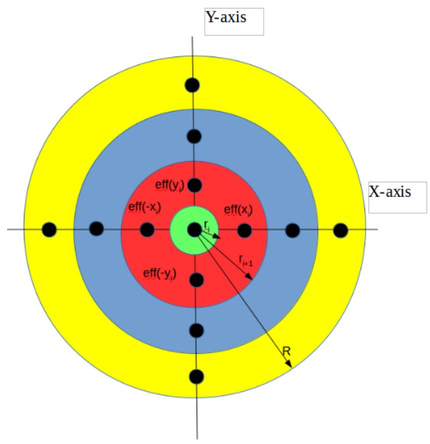

FIGURE 3.14: Diagram demonstrates how the efficiency was integrated analytically.

$$\epsilon_0 \times \left(\frac{r_0^2}{R^2}\right) + \sum_{i=0}^{7} \frac{\left(\epsilon\left(x_i\right) + \epsilon\left(-x_i\right) + \epsilon\left(y_i\right) + \epsilon\left(-y_i\right)\right)}{4} \times \frac{r_{i+1}^2 - r_i^2}{R^2} \tag{3.1}$$

Where ϵ_0 is the efficiency at the point (0,0) the center at, r_0 = 1mm, and ϵ_i is the efficiency at the disc between the circle with r_{i+1} and r_i, where i is the circle number, R is the radius of the big circle for FOT R=15 mm.

Observed Features of the FOT

The FOT output light does not diverge or scatter over the surface but it shows 1-to-1 mapping with magnification, or demagnification if the light moves from the small base to the bigger one, or when the light goes from the big base to the small one respectively, see Figure (3.15).

FOT big base view

FOT small base

FIGURE 3.15: The output light from the 2 bases of the FOT.

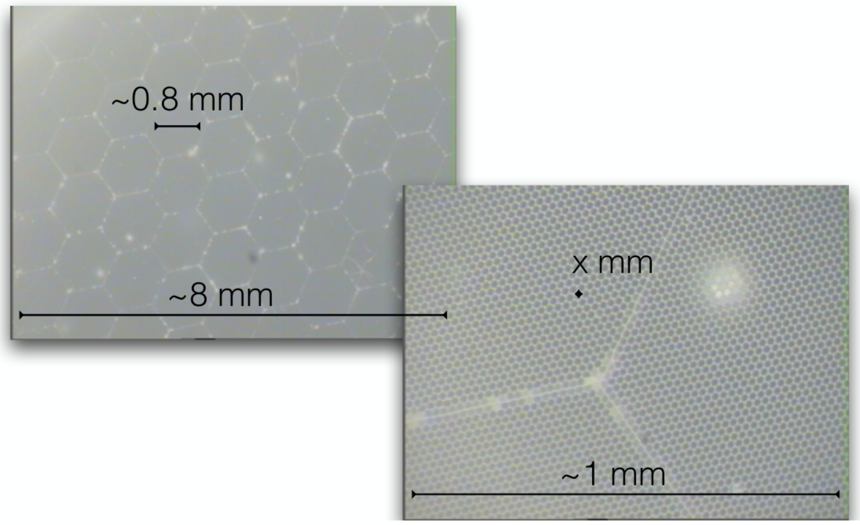

FIGURE 3.16: A microscopic picture for the big base of the FOT.

Microscopic pictures of the FOT show its internal structure, as compressed fiber, this explains the reason of less efficiency at the peripherals than at the center, because the fiber is longer and more bent at the peripheral than at the center which is shorter and straight, Figure (3.16), Figure (3.17).

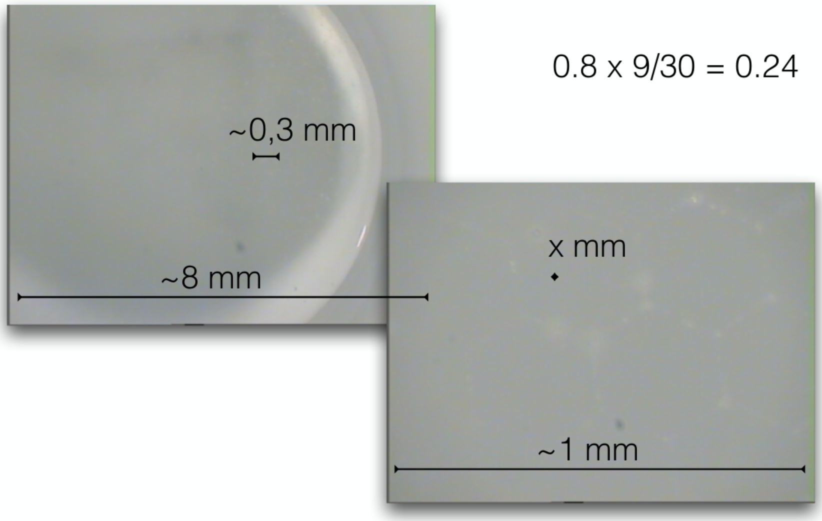

FIGURE 3.17: A microscopic picture for the small base of the FOT (photo taken by K.Suzuki).

3.4.3 Testing the Total Efficiency of the FOT and Light Guide Using LED.

The measurement as described in Section (3.4.1) was performed again to compare the light transmission efficiency of the plastic light guide and the FOT under the same condition. The same setup was used in Section (3.4.1) just a few parameters were changed. The distance from the LED to the light diffuser is 50 mm, the distance from the light diffuser to the PMT is 100 mm. For this parameters, the total efficiency of the plastic light concentrator and the FOT is calculated from the measurements in Table (A.14). **The efficiency of the Light guide** = $(73.07 \pm 0.13)\%$, **the efficiency of FOT** = $(45.24 \pm 0.04)\%$.

3.4.4 Total Light Efficiency of the FOT and Light Guide With Laser

The LED was replaced by a Laser (PiL040X Laser from advanced Laser diode systems). It has a wavelength of (405 $\pm$15) nm and has a pulse width of less than 45 ps. The fiber has a 25^o acceptance angle. The distance between the Laser to the light diffuser is 50 mm and the distance from the light diffuser to the PMT is 90 mm. The measured data listed in Table (A.4). **The efficiency of Light guide**= (83.39 ± 0.13)%, **the efficiency F OT** = (10.01 ± 0.23)%.

3.4.5 Position Efficiency of the FOT and the Light Guide With Laser

The same setup as in Section(3.4.2), only the light source was replaced by be Laser, the plastic cover has 7 holes for each in the direction of x-axis and y-axis. The diameter of each slot changed to be 3 mm and the distance between two adjacent holes is 1 mm, the distance from the lateral side to the 1st slot is 1.5 mm. The pulse height of the PMT coupled to FOT was determined at each point and divided by the measured reference value (without the light concentrator). The applied voltage to the PMT is 1750V. Optical grease was added for at each step between the optical fiber and the PMT. The results of the plastic light guide is listed in Table (A.5). The FOT results listed in Table (A.6), see also Figure (3.18) and Figure(3.19). Equation (3.2) can be applied to determine the average efficiency: **Efficiency of the Light guide** = (70.51 ± 0.33)%, **efficiency of the FOT** = (9.05 ± 0.59)%.

$$\epsilon_0 \times \left(\frac{r_0^2}{R^2}\right) + \sum_{i=0}^{3} \frac{(\epsilon(x_i) + \epsilon(-x_i) + \epsilon(y_i) + \epsilon(-y_i))}{4} \times \frac{r_{i+1}^2 - r_i^2}{R^2} \tag{3.2}$$

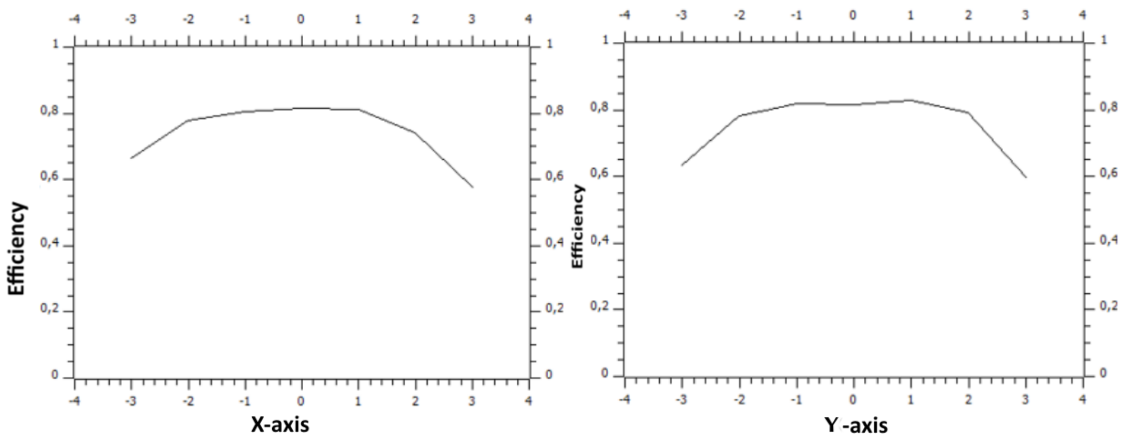

FIGURE 3.18: The position efficiency of the plastic light guide along the x-axis and the y-axis (Andreas Lanz).

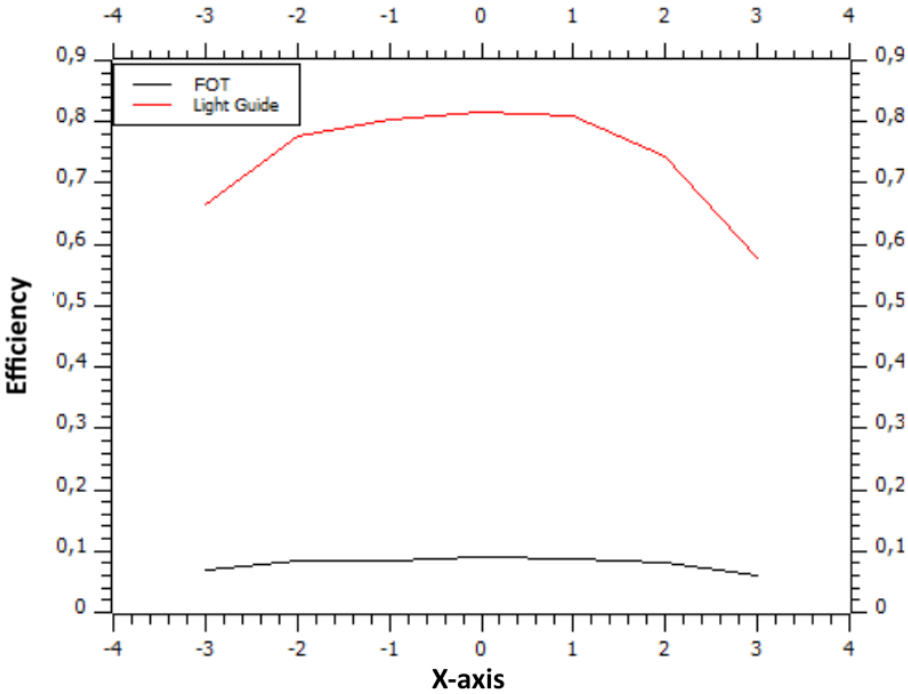

FIGURE 3.19: The position efficiency of the FOT and the Light Guide along the x-axis (Andreas Lanz).

3.5 Photosensor

Three types of photosensors were tested with this optical fiber bundle, in order to decide which one could be used for the V0+ detector.

1. Silicon Photomultiplier (SiPM).
2. Photomultiplier Tube (PMT).
3. Microchannel Plate Detector (MCP-PMT).

"**General properties of photon detectors:** Photon detectors are characterized by the following properties:

- Quantum efficiency (QE): The probability that incident photon generates a photo-electron.

- Collection efficiency (CE): The probability that the photoelectron starts the electron amplification.
- Gain (G): The ratio between the output current of the photodetector to the current produced by the incident photons on the detectors.
- Dark current or dark noise: The electrical signal with no photon at the input.
- Dynamic range: The minimum-maximum signal range available from the detector.
- Time dependence of the response: This includes the transit time, which is the time between the arrival of the photon and the electrical pulse, and the transit time spread (TTS), which contributes to the pulse rise time and duration.
- Single photon detection capability: Important when measuring very low level light intensities.
- Rate capability: Inversely proportional to the time needed, after the arrival of one photon, to get ready to receive the next (i.e. recovery time).
- Stability: Essential for long term operation at elevated counting rates." cited from [21]

We focused mostly in our measurement on the SiPM as it is cheaper and has very low bias voltage in comparison to other alternatives.

3.5.1 MPPC (Multi-Pixel Photon Counter) or SiPM (Silicon Photomultiplier)

"The MPPC (multi-pixel photon counter) is a sensitive opto-semiconductor device sometimes also called silicon photomultipliers (SiPM). It is a photodetector device using multiple APD (avalanche photodiode) pixels operating in Geiger mode [22]" cited from [23]. "The SiPM gives a high photon-counting capability and can be used to detect a single photon. Nowadays, SiPM has various applications including medical diagnosis, academic research. The SiPM operates on a low bias voltage and provides a high multiplication ratio (gain), high photon detection efficiency, fast response, good time resolution, and operates over a wide spectral response range, so it gives the high-performance level which is needed for photon counting. The SiPM is immune to magnetic fields, highly resistant to mechanical shocks, and does not suffer from "burn-in" by incident light saturation." cited from [23].

The V0+ detector requires high efficiency, high dynamic range (1 – 500) particles, radiation hardness and must be compatible with 25 ns bunch spacing and 1-2 MHz interaction rate for pp collisions of the new LHC operation, while keeping the time resolution of about 200 ps. In order to comply with this condition the photosensor should meet the following features:

1. Recovery time should be < 25 ns.
2. It should stand for average rate of 1-2 MHz.
3. It should have a high dynamic range.
4. Good time resolution 200 ps.

From the digitized waveform taking during the beam time in October 2015, the rise time for KETEK SiPM 6x6 mm^2 with Photonique AMP-0604 preamplifier was 13 ns, this signal is pretty slow to meet the requirements of the V0+ detector. Several measurements were performed in order to optimize the rise time of the SiPM signal.

Test #1:

The rise time of the KETEK SiPM PM6606 6x6 mm^2 with Photonique AMP-0604 [3] preamplifier was measured, Figure (3.20). 28.3 V was the applied bias voltage to the SiPM and 5 V to the preamplifier. The SiPM was exposed to a beam of laser light. The output signal was monitored using an oscilloscope. The measured rise time was 5.1 ns and full

[3] Photonique AMP-0604: Advantech UK supplies Photonique Charge Sensitive Preamplifiers tailored for use with SiPMs (Silicon Photomultipliers), including those supplied by Sensl, Hamamatsu (MCCP), Ketek etc [24]. These devices are compact in size, allow the bias voltage to be set on the SiPM and enable the gain to be set through adjustment of the supply voltage to the board.

width at half maximum (FWHM) of 56.5 ns Figure (3.21). The signal is rather slow to meet the requirements of V0+ detector.

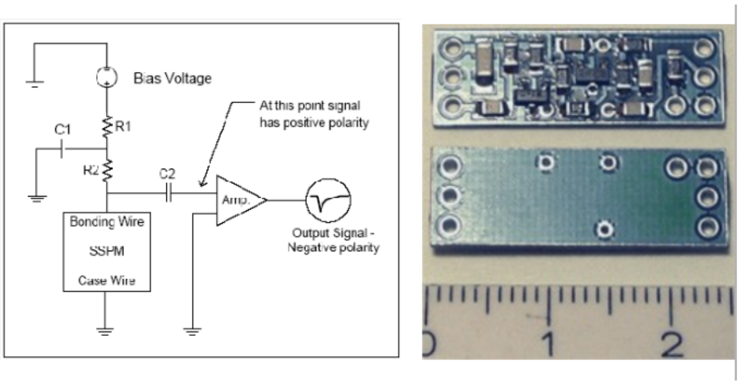

FIGURE 3.20: The adjacent diagram is a functional schematic of the AMP-0604 circuits [24].

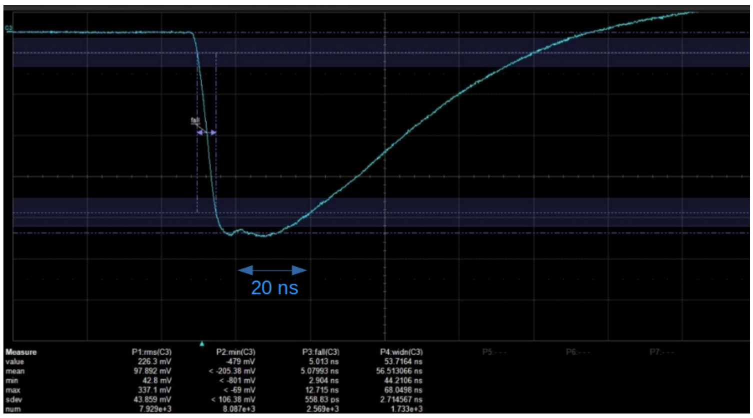

FIGURE 3.21: The output signal of the KETEK 6x6 mm^2 with Photonique AMP-0604 preamplifier.

Test #2:

The Photonique AMP-0604 preamplifier was replaced by PSI voltage preamplifier [25], Figure (3.22). The output signal was definitely better with rise time = 1.2 ns and (FWHM)= 3.6 ns, Figure (3.23).

An alternative solution was to skip the preamplifier and use the recommended circuit Figure (3.24) from the KETEK data sheet [17] in order to improve the rise time. Equation (3.3) demonstrate how to calculate the rise time.

$$\sigma = \sqrt{\sigma^2_{sci+fibers} + \sigma^2_{preamp} + \sigma^2_{sensor}} \tag{3.3}$$

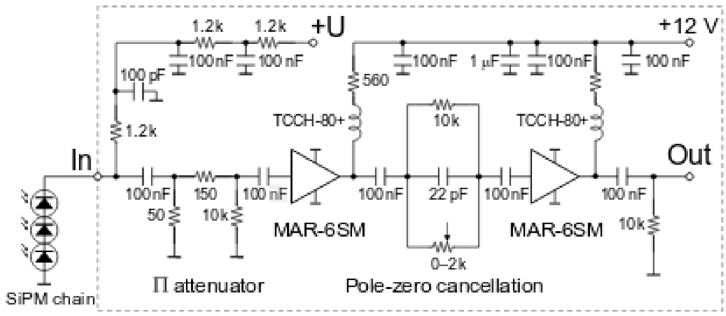

FIGURE 3.22: Circuit diagram of the amplifier board [25].

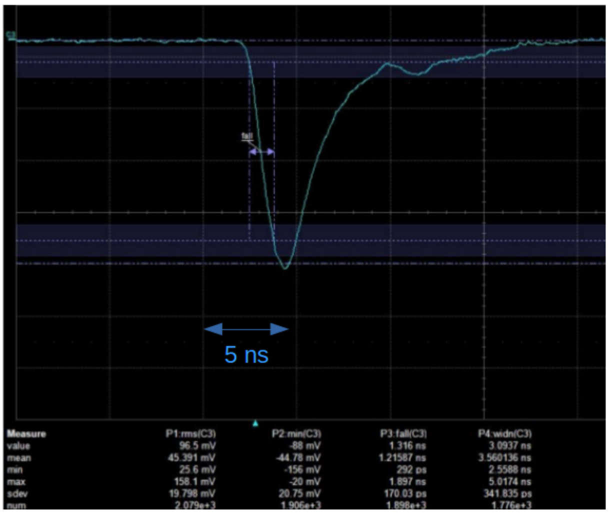

FIGURE 3.23: The output signal of the KETEK 6x6 mm^2 with PSI voltage preamplifier.

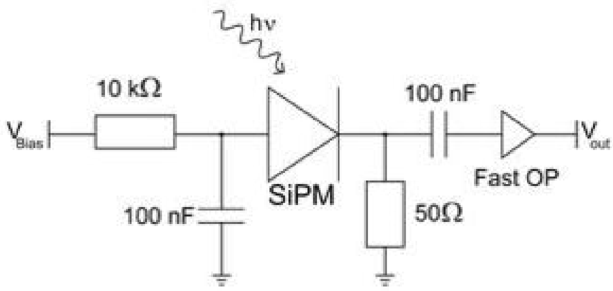

FIGURE 3.24: The KETEK Silicon Photomultiplier read out circuit.

Test # 3:

The setup is shown in Figure (3.25). The circuit in Figure (3.24) was used with the SiPM, only the preamplifier was skipped from the circuit. The SiPM was exposed to light coming from a single mode optical fiber and this fiber is coupled to the laser, as shown in Figure (3.25). The cables and the fiber were routed inside the box through an aperture, these apertures were closed completely by a clay.

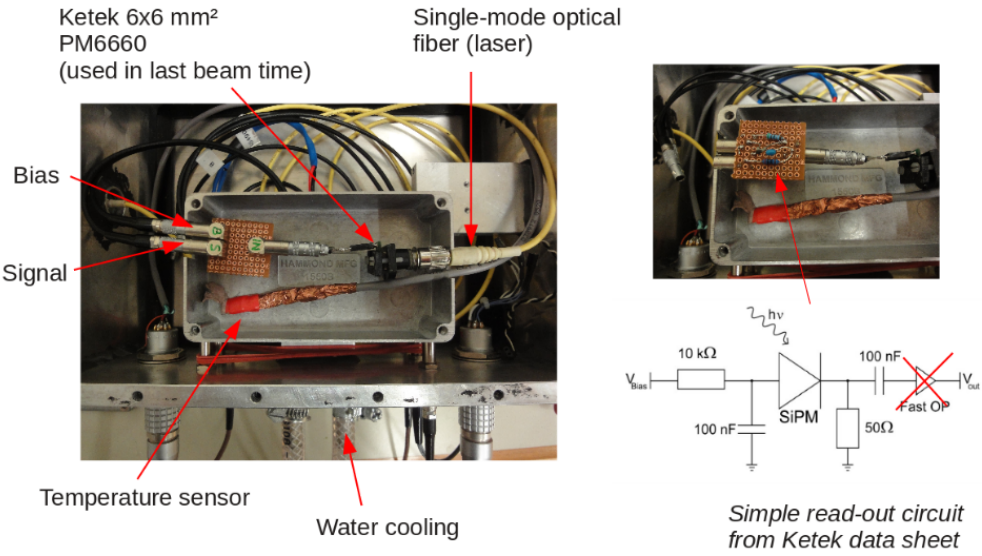

FIGURE 3.25: The new setup for the read out circuit.

The circuit has a low pass filter 100 nF + protective resistor 10 kΩ, the applied bias voltage to the SiPM is 28.3 V. The output signal has a fast rise time of 2.5 ns but still has a long tail, with a signal width (FWHM) of 116.5 ns, pulse height of 34.3 mV with a current of 30 μA, Figure (3.26).

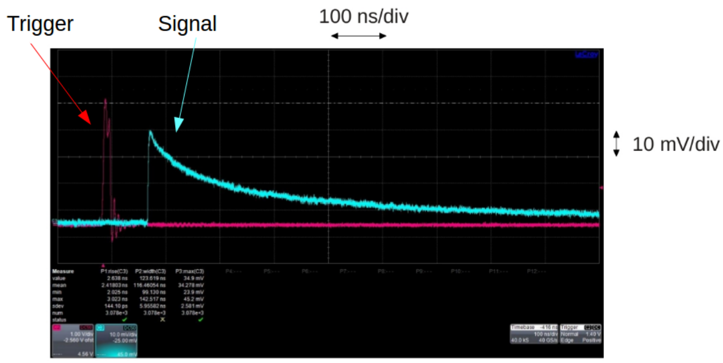

FIGURE 3.26: The read out signal using the KETEK SiPM without preamplifier.

Test #4:

The circuit was adjusted again to reduce the value of one capacitor to be 22 pF instead of 100 nF, Figure (3.27), in order to reduce the value of the time constant to get a faster signal, However, the gain will be reduced. The applied bias voltage was the same 28.3V.

The obtained signal from this test shows a rise time 1.2 ns, fall time 20 ns, signal width (FWHM) 11.8 ns, pulse height 26.5 mV, with measured current of 30 μA Figure (3.28).

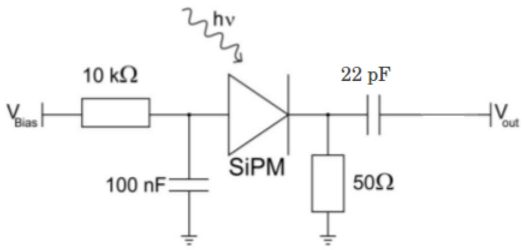

FIGURE 3.27: The read out circuit using 22 pF instead of 100 nF without preamplifier.

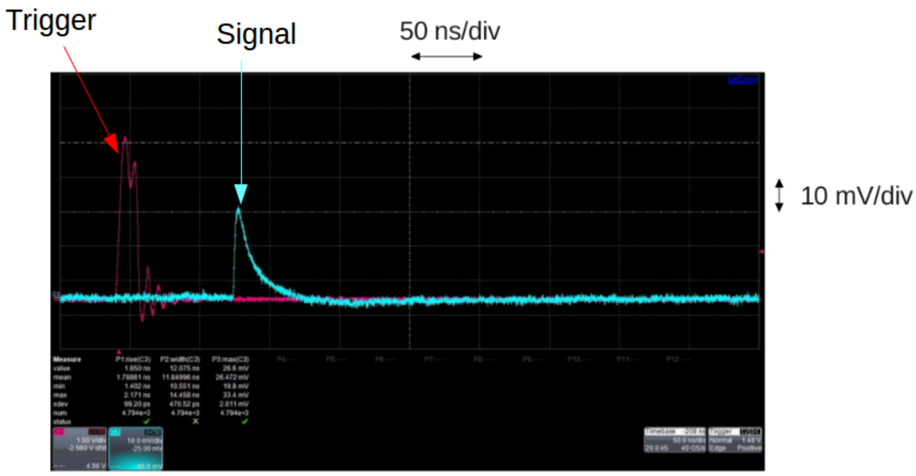

FIGURE 3.28: The read out signal using the circuit of Fig.(3.27).

Test #5:

The circuit was adjusted again by reducing the loading resistor to be 1kΩ instead of 10 kΩ as shown in Figure (3.29.), with an applied bias voltage of 28.3 V.

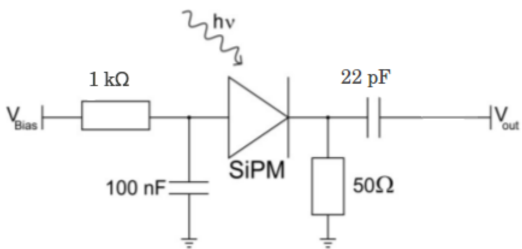

FIGURE 3.29: The read out circuit with loading resistor to be 1k Ω instead of 10 kΩ without Preamplifier.

The output signal from this circuit has a rise time of 1.8 ns, a fall time of 20 ns,a signal width (FWHM) of 11.7 ns, a pulse height of 30.1 mV, with a current of 49 μA, Figure (3.30). Using the circuit in Figure (3.29) leads to a lower gain and the produced current turns to be high. The SiPM is a low-level light detector, so a high light input results a large current flow and may cause a large voltage drop on the protective resistor, so the circuit needs always to be adapted to the application.

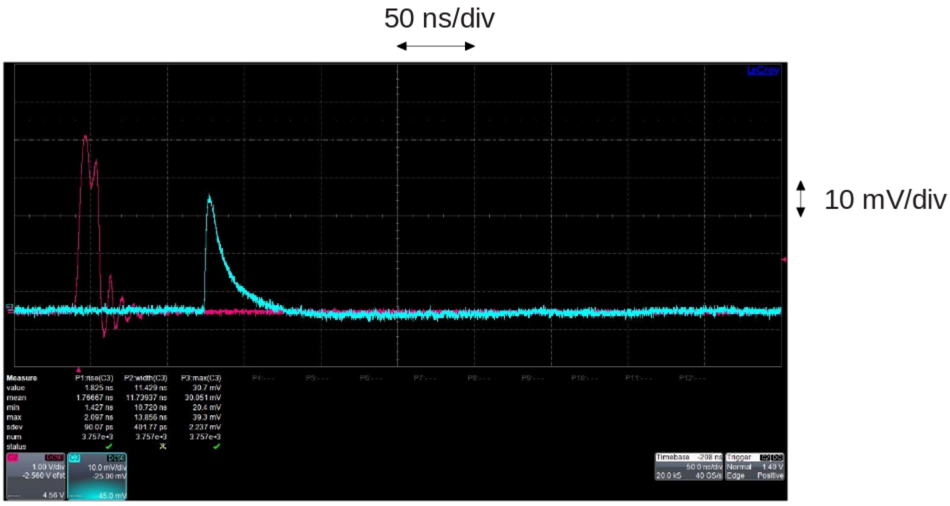

FIGURE 3.30: The read out signal using circuit in Figure (3.29).

Test #6:

The capacitor was adjusted once again to be 15 pF instead of 22 pF as in Figure (3.31) and we applied 28.3 V bias voltage to the SiPM.

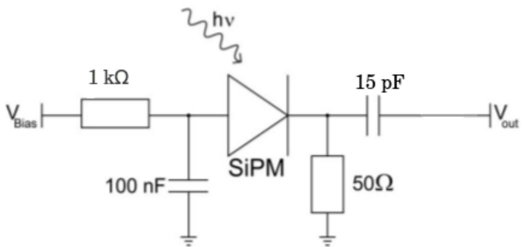

FIGURE 3.31: The read out circuit using loading resistor 1kΩ and 15 pF instead of 22 pF without preamplifier.

The output signal has now a rise time of 0.8 ns, a fall time of 2.1 ns, signal width (FWHM) of 2.6 ns, a pulse height 13.4 mV, and a current 49 of μA, Figure (3.32).

When the bias voltage was increased to 30.0 V the rise time is 0.9 ns, the fall time 2.3 ns, the fall width (FWHM) 2.6 ns, the pulse height 24.1 mV and the current 496 μA. Increasing the bias voltage leads to increase the current especially when the protective resistor is small.

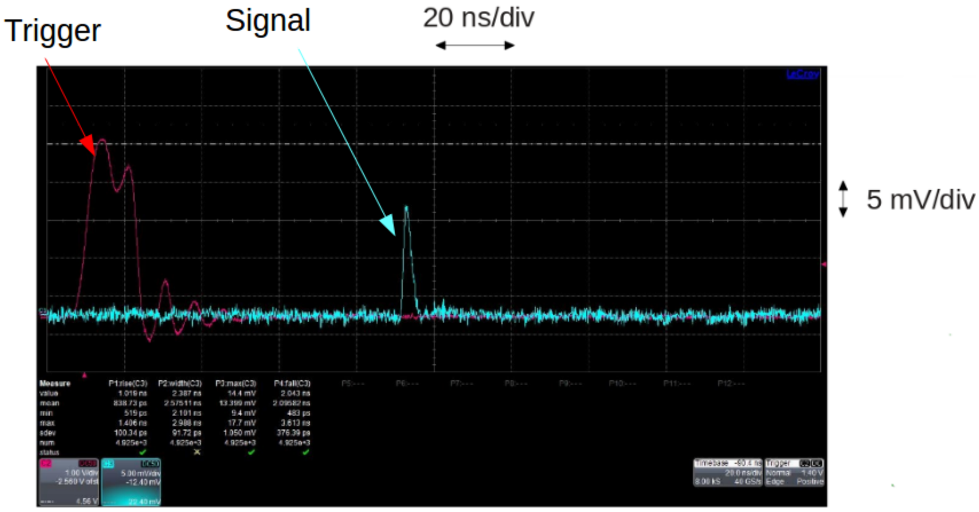

FIGURE 3.32: The read out signal using circuit in Figure (3.31).

Test #7:

The AC coupling (high pass filter) was skipped as shown in Figure (3.33). The applied bias voltage was 28 V.

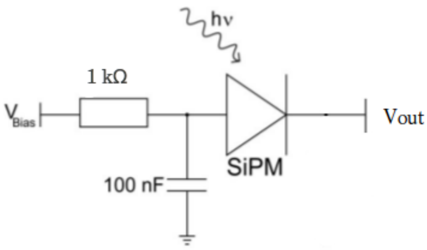

FIGURE 3.33: The read out circuit using DC coupling instead of AC coupling without preamplifier.

The obtained signal shows rise time of 2.4 ns, fall time of 1.2 μs, signal width (FWHM) of 213.3 ns, and the pulse height 59 mV Figure (3.34). The AC coupling gives a faster signal than DC with (FWHM) of 2.6 ns and it turns out to be a better choice to be used with the SiPM.

Test #8:

The circuit in Figure (3.33) was connected now to the Hamamatsu SiPM 6x6 mm^2 at a bias voltage of 58 V, see Figure (3.35), the measured rise time is 1.7 ns and the fall time is 219 ns. Hamamatsu SiPM 6x6 mm^2 gives a faster rise time than one achieved with a KETEK SiPM.

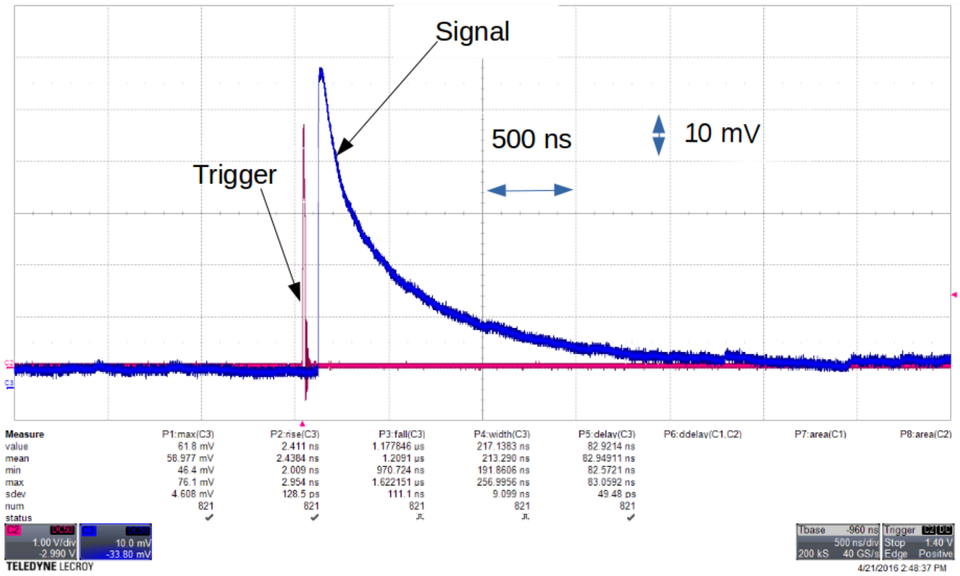

FIGURE 3.34: The read out signal using circuit in Figure (3.33).

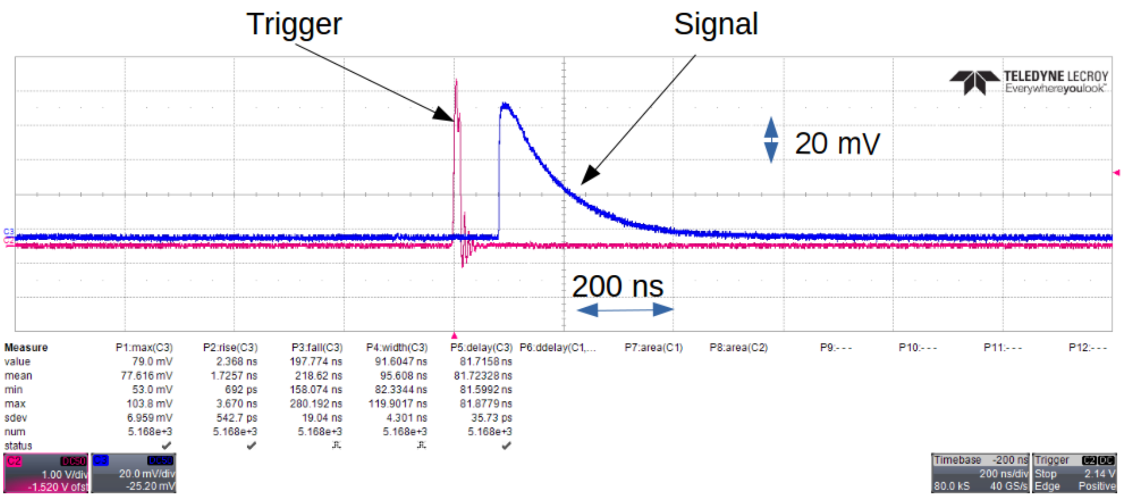

FIGURE 3.35: The read out signal from Hamamatsu SiPM (S13360-3025PE)) 6x6 mm^2 using DC coupling instead of AC coupling without Preamplifier.

Adding the circuit Figure (3.31) to the SiPM Hamamatsu 6x6 mm^2, the measured rise time is 1 ns and the fall time is 2.3 ns. Figure (3.36).

Testing the Rate Capability of SiPMs

The amplitude of the SiPM signal at different frequencies was measured by exposing the SiPM to 300 photons, (these 300 photons were just a preliminary expectation on how many photons will be produced per MIP).

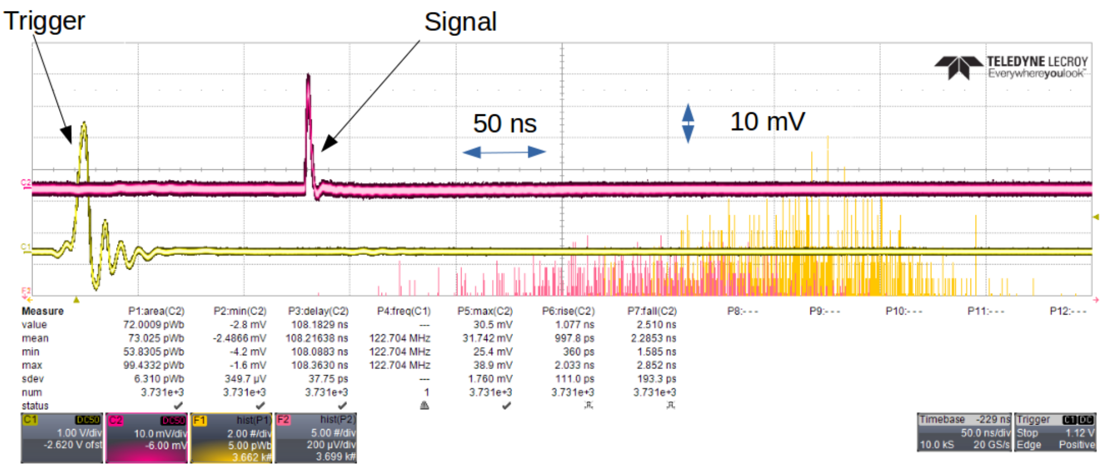

FIGURE 3.36: The read out signal from Hamamatsu 6x6 mm^2 using AC coupling with no Preamplifier, as in Figure (3.31).

Photon counting measurement and analysis approach: the oscilloscope histogram shows the discrete nature of the SiPM output, Figure (3.39). The difference between 2 adjacent peaks in the histogram shown in the Figure (3.39) represents one photon count p.e.. The purpose of using the preamplifier is to see the difference between the peaks clearly, then we remove it to carry out the measurement with the nominated circuit in Figure (3.31).

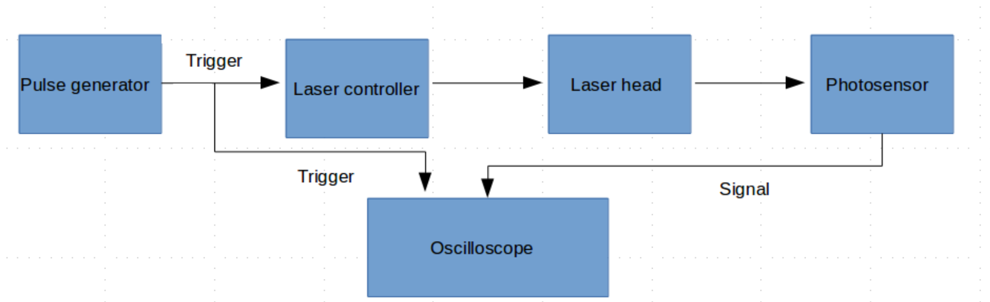

FIGURE 3.37: A scheme of the setup for testing the rate capability.

Experimental setup: is shown in Figure (3.38) and Figure (3.37). One optical fiber connected to the laser, Hamamatsu 6x6 mm^2 SiPM, with bias voltage of 54 V, the used preamplifier is a fast photonic with amplification factor 23 with a bias voltage of 5 V. These components were fixed in the same position so the light intensity could not change when the preamplifier get replaced by the nominated circuit.

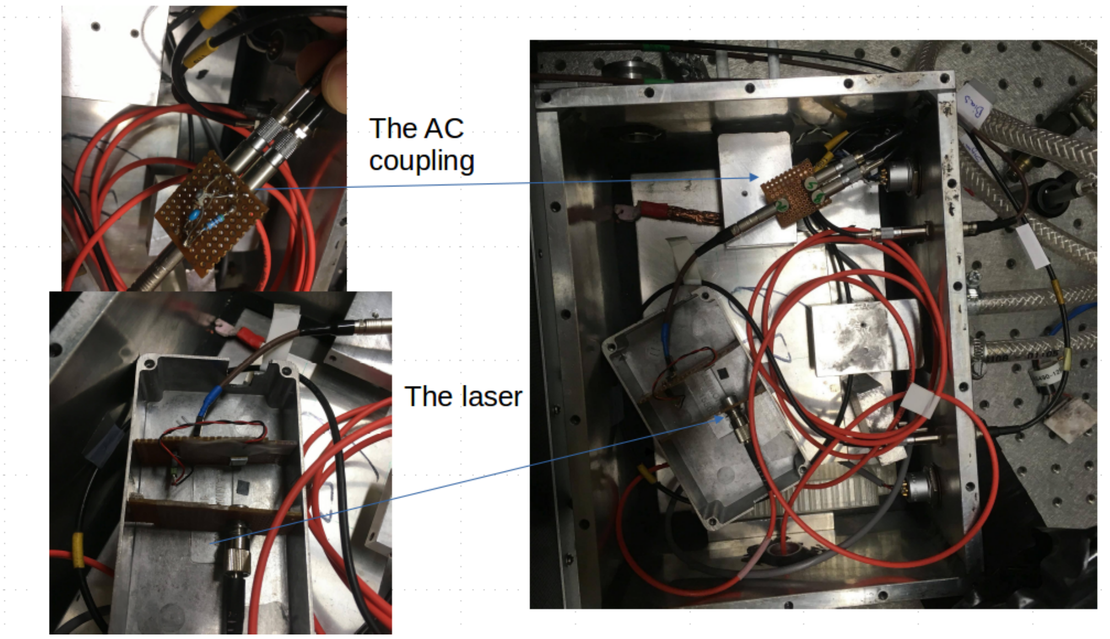

FIGURE 3.38: The setup for testing the rate capability when 300 photons hit the SiPM.

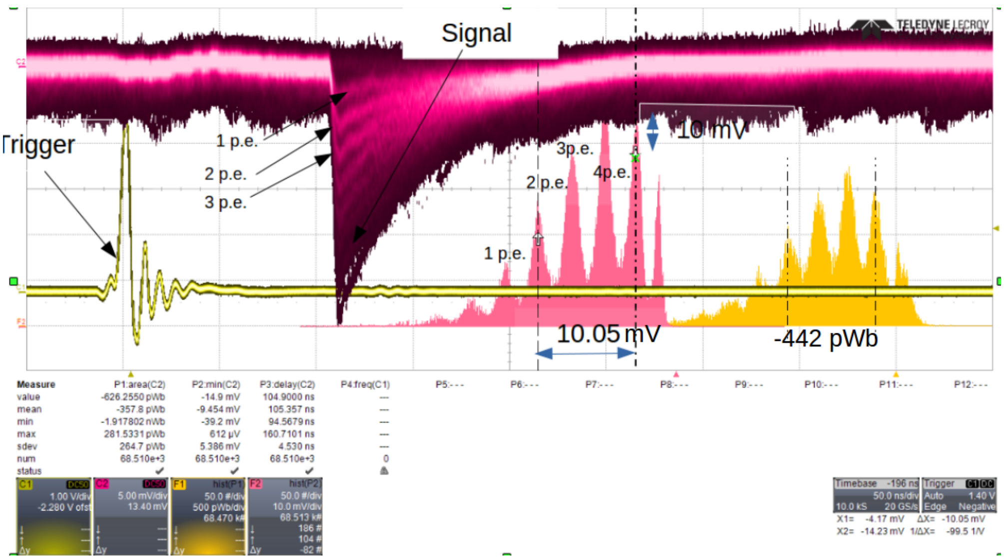

FIGURE 3.39: Oscilloscope finger spectra of Hamamatsu 6x6 mm^2 SiPM.

The difference between 2 adjacent magnified peaks = 3.34 mV, see Figure (3.39). The amount of light was adjusted to reach a signal height of 1002 mV. Then the preamp was removed and the nominated circuit was added. Then pulse amplitude was measured at different frequencies, the results are listed in Table (A.7). The signal at 1 MHz dropped to 80 % of its value at 1 kHz, Figure (3.40).

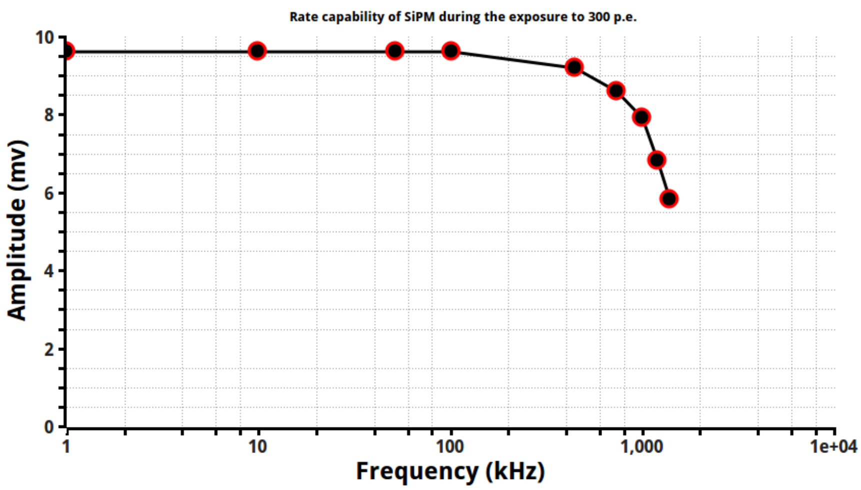

FIGURE 3.40: Frequency vs signal amplitude at 300 photons hit the SiPM.

The rate capability was determined at 2 different bias voltage using the nominated circuit. The results are shown in Table (A.8). It is clear that at low bias voltage the rate capability is much better as the bias voltage increases, the junction capacitance increases and this leads to a longer time constant. In case of 54 V applied bias voltage, the signal amplitude at 1 MHz, is ~ 76 % of its value at 1 kHz, however, at a bias voltage of 55 V the signal amplitude is only $\sim 48\%$ of its value at 1 kHz, see Figure (3.41).

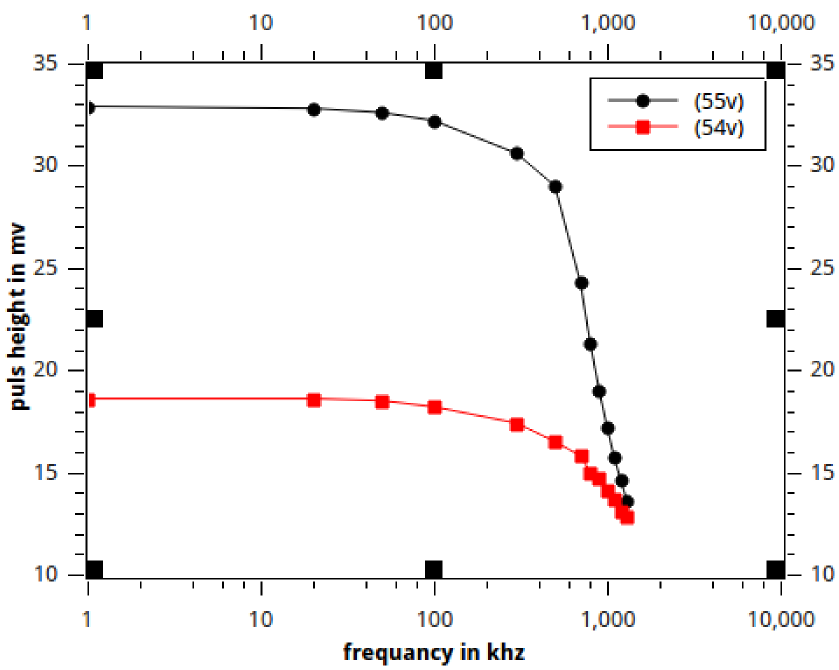

FIGURE 3.41: Frequency vs signal amplitude at 54 V and 55 V bias voltage.

This could be attributed to the junction capacitance of the SiPM. The junction capacitance is a function of the applied bias voltage, at the higher the bias voltage the higher the junction capacitance.

3.5.2 Photomultiplier Tube (PMT)

"The photomultipliers are the most widely used photosensor, they have been used to detect low amount light in the UV to the visible range, high-energy photons (X-rays and gamma rays) and ionizing particles. Nowadays, the photomultiplier tube (PMT) remains in the forefront in light detection" cited from [26]. "It is a vacuum tube consisting of an input window, a photocathode, focusing electrodes, an electron multiplier and an anode usually sealed into an evacuated glass tube. Figure (3.42) shows the schematic construction of a photomultiplier tube" cited from [27].

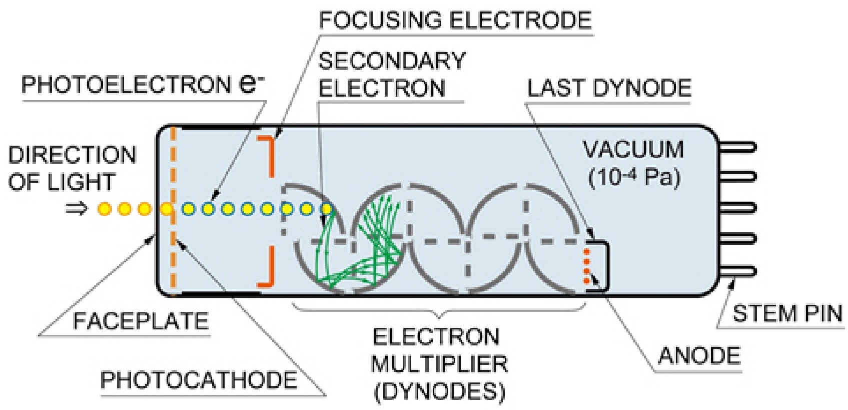

FIGURE 3.42: A scheme of the main elements of a photomultiplier [28].

"Photomultiplier operation The light which enters the photomultiplier tube will be detected and gives an output signal through the following processes:

- Light passes through the input window.
- A cathode coated with a material of low work function, based on the principle of photoelectric effect or photoemission. When a photon with energy higher than the work function hits the cathode it liberates an electron [29].

- Photoelectrons are accelerated and focused by the focusing electrode onto the first dynode where they get multiplied by a secondary electron emission. This secondary emission will be repeated at each of the successive dynodes.
- High voltage power supply is need to produce an electric field between the cathode and the dynodes.
- The multiplied secondary electrons emitted from the last dynode are finally collected by the anode to be read by a current meter" cited from [27].

3.5.3 Rate Capability of PMT

The measurement was done by exposing a Fine-mesh PMT H8409-70 to laser light, the pulse height was determined at different frequencies using an external trigger for the laser. The experimental setup is the same as in Figure (3.37). The measurements were performed at 2 different frequencies and at bias voltage 1600 V and 1800 V. The results are listed in Table (A.9). The result shows that the PMT is more stable than SiPM at higher frequencies, see Figure (3.43). The signal value at MHz is reduced to 88 % and 92% at 1600 V and 1800 V respectively compared to its value at 50 kHz.

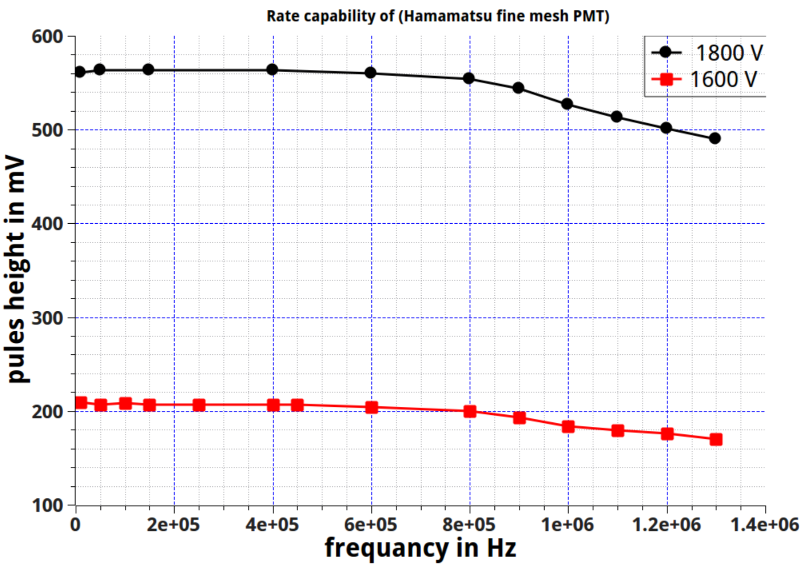

FIGURE 3.43: Frequency vs signal amplitude of Fine-mesh PMT.

3.5.4 Micro-channel Plate (MCP-PMT)

"Micro-channel plate (MCP) is an electron multiplier that used for particles detection (electrons or ions). It has the ability to detect and operates over a wide range of a spectrum (from ultraviolet radiation to X-rays). The common feature between PMT and MCP, that both amplify the single particles or photons by the multiplication of electrons via secondary electron emission. As a result of having several channels, MCP-PMT is able to provide spatial resolution" cited from [30].

FIGURE 3.44: Photonis Planacon 85012 MCP-PMT [31].

"A micro-channel plate (MCP-PMT) consists of a two-dimensional array with plenty number of microchannels (made of glass capillaries). The channels are parallel to each other with diameter of $\sim$ 10 micrometers, the space between channels $\sim$ 10 micrometers, thier inner walls have an electrical resistance and secondary emissive properties, each channel behaves as an individual electron multiplier, this amplification takes place under high electric field. The channels are bundled to form a slab of 2 millimeter thickness" cited from [27] [32].

Operating Mode

"When a primary electron hits the inner wall of a channel, secondary electrons are emitted and accelerated by the electric field created by the applied voltage between the ends of the MCP, these secondary electrons hit the channel wall again to produce additional electrons.

The process is repeated many times across the channel and as a result, a large number of electrons are released" cited from [27].

Chapter 4

Results and Data Analysis of the Beam Times in 2016

4.1 Introduction

In this chapter, the results and the data analysis are discussed. This data was taken during the beam times in June 2016, and October 2016. Both beam times were conducted at the T10 east experimental area at the PS facility in CERN, Different model and design of fiber bundles were tested with 2 different scintillator material, light concentrators, and photosensors.

The experimental setup was the same setup as in Figure (2.5). CAEN desktop waveform digitizer and CAEN WaveDump software were used for data acquisition [33]. All the data was analyzed by using ROOT framework [34].

4.2 Beam Time June 2016

DAQ started from June 14, 2016, till June 22, 2016, more than 65 runs. Combinations of detector parameters were tested as shown in the schematic configuration in Figure (3.2) and mostly A and B configurations were tested. The tested components during June beam time are listed in Table (A.10). In order to make the plotting easier and more comprehensive, a cryptic symbols or abbreviations were giving to each component to denote the component and the configuration of the detector. This abbreviations are listed in Tables (A.11), (A.12), (A.13), and (A.14).

4.2.1 Scintillator Results and Comparison

Two different scintillator materials were tested with several different configurations, see Figure(4.1).

- EJ-204 gives mostly more light than EJ-228.
- The achieved time resolution is generally also better with EJ-204 (except only Asahi fiber bundle, where EJ-228 gave a slightly better time resolution than EJ-204.
- The best measured time resolution was the combination of (EJ-204 + Kuraray fiber + FM-PMT) $\sigma \sim 210$ ps.

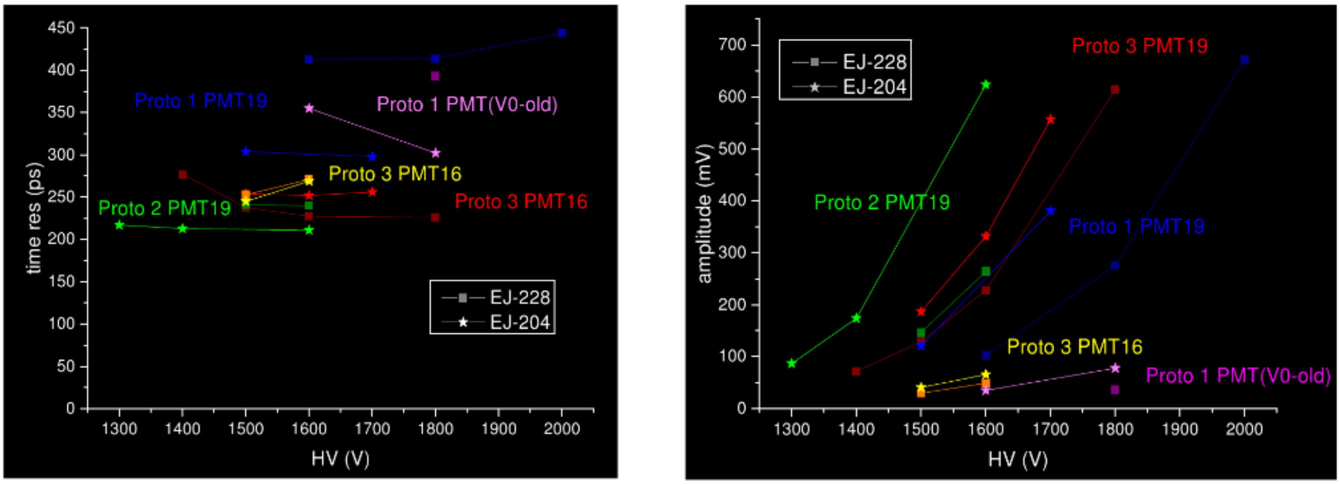

FIGURE 4.1: Comparison between the scintillator time resolution and signal amplitude

4.2.2 Fiber Results and Comparison

Different types of fibers as well have been tested in several configurations with different scintillator materials and photosensors, Figure (4.2).

- Best results obtained with Kuraray round fiber (Proto2). $\sigma \sim 210$ ps.

- Asahi round fibers (Proto3) gives relatively good results with the configuration (EJ-228 + Asahi fiber + FM-PMT). $\sigma \sim 231$ ps.

- Best time resolution is the configuration of (EJ-204 + Kuraray fiber + FM-PMT): $\sigma \sim 210$ ps.

- Bicron square fiber bundle shows the worse time resolution and low amplitude.

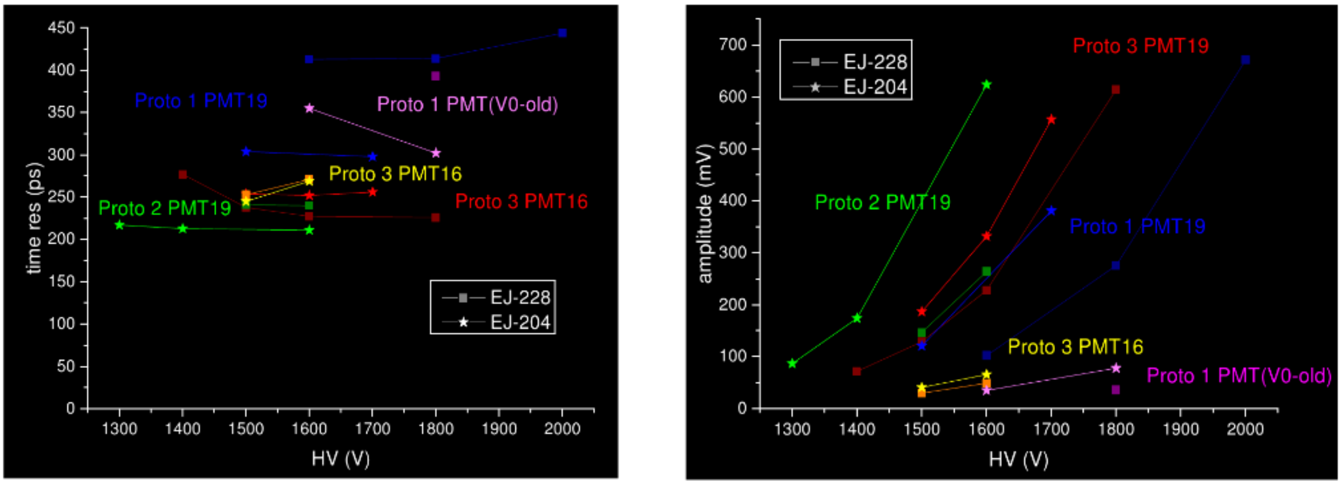

FIGURE 4.2: Comparison between the fiber bundle time resolution and signal amplitude

4.2.3 Photo-detector Results and Comparison

Fine-mesh PMTs (16 and 19 stages), MCP-PMT and SiPMs have been tested also in different combination with scintillator materials and fiber bundles, Figure (4.3).

- The best results were obtained with fine-mesh PMTs: $\sigma \sim 210$ ps.

- The two models of the PMTs (16 and 19) give almost the same time resolution.

- FM-PMT (19 stages) had about 5 times higher gain at same applied bias voltage.

- SiPM gave $\sigma \sim 314$ ps with PSI preamplifier. The nominated circuit in Figure (3.31) with no preamplifier gives time resolution of $\sigma \sim 350$ ps.

- Best results were obtained with fine-mesh PMTs: $\sigma \sim 210$ ps.

- When the signal amplitude goes beyond 80 mV, the time resolution gets saturated Figure(4.4).

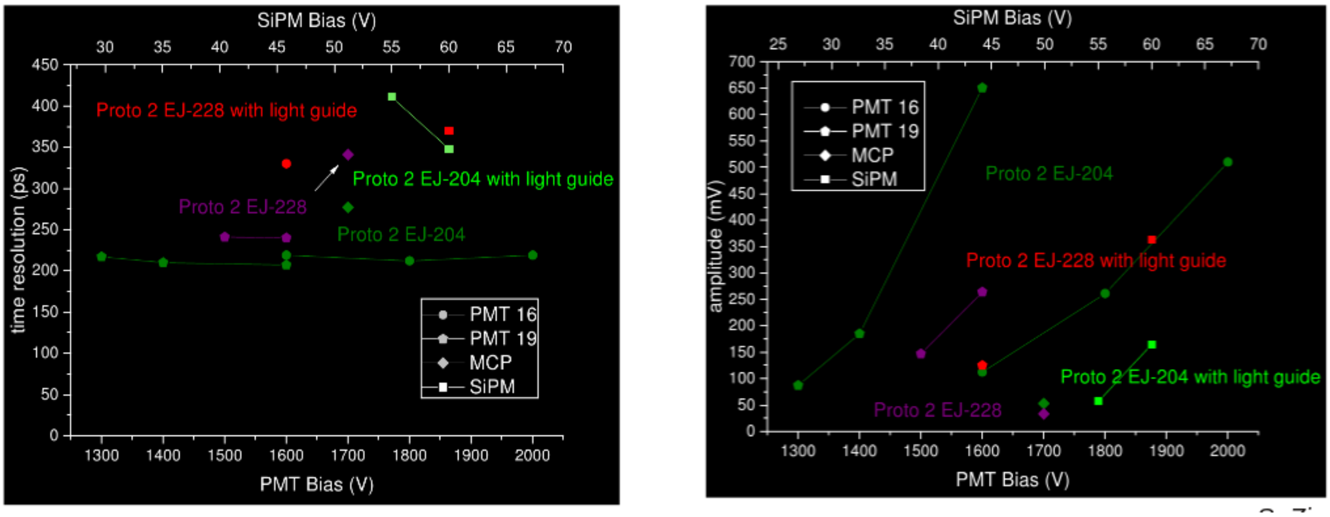

FIGURE 4.3: Comparison between the photo-sesnors time resolution and Signal amplitude.

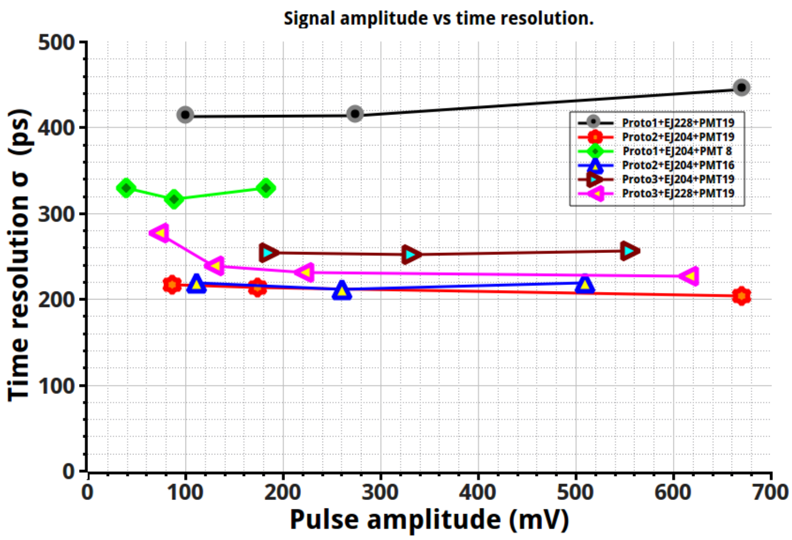

FIGURE 4.4: Signal amplitude vs time resolution.

4.2.4 Light Guide Results and Comparison

Different types of light concentrators in different sizes and shapes were tested during the beam time, see Figure (4.5).

- Pyramid-shaped light guides show generally better performance than conical guides.

Name	Type	Shape	∅ (IN)	∅ (OUT)	Ratio (area)	Ratio (linear)	Transmission	Time resolution
FOT	Taper	-	30	9	11.1	3.3	~ 27%	factor 2.1 worse
LGV1a	Light guide	conical	30	9	11.1	3.3	~ 27%	factor 2.1 worse
LGV2	Light guide	conical	22.5	7	10.3	3.2	~ 30%	factor 1.8 worse
LGM1	Light guide	pyramid	22	11	4	2	~ 90%	approx. same
LGM3	Light guide	pyramid	21	6	12.3	3.5	~ 50%	factor 1.4 worse

FIGURE 4.5: Comparison between a different light concentrator and their impact on the gian and the time resolution.

- Linear reduction factor 2 (factor 4 in the area) does not deteriorate the detector prototype performance.
- FOT shows a bad performance due to poor light transmission.
- Higher reduction factors have a significant impact on the obtained time resolution and efficiency.

4.3 Beam Time October 2016

DAQ started from October 26, 2016, until November 2, 2016, October 26, 2016, until November 2, 2016, more than 40 runs were performed during this beam time. Only 2 fiber bundles Kuraray (proto2), which showed the best performance during June beam time, and Mitsubishi Rayon (proto5), a new fiber bundle that was prepared by a Japanese company. Two photodetectors (PMT19 and MCP-PMT) were tested during this beam time as the SiPM option was discarded after June beam time. The main goal was to increase the dynamic range up to 500 particles as the maximum readout of the FIT electronics is 5 V. In order to comply with this condition, the signal amplitude of the photosensor should not exceed 10 mV per MIP while keeping a good time resolution.

4.3.1 Stability of Optical Connection With Grease

All the photosensors scintillator are attached to fibers using optical grease, so it was important to test its stability as well. The fibers were kept coupled to the scintillator and the photosensor with Saint-Gobain crystals silicone grease since the last beam time in June 2016, Figure (4.6).

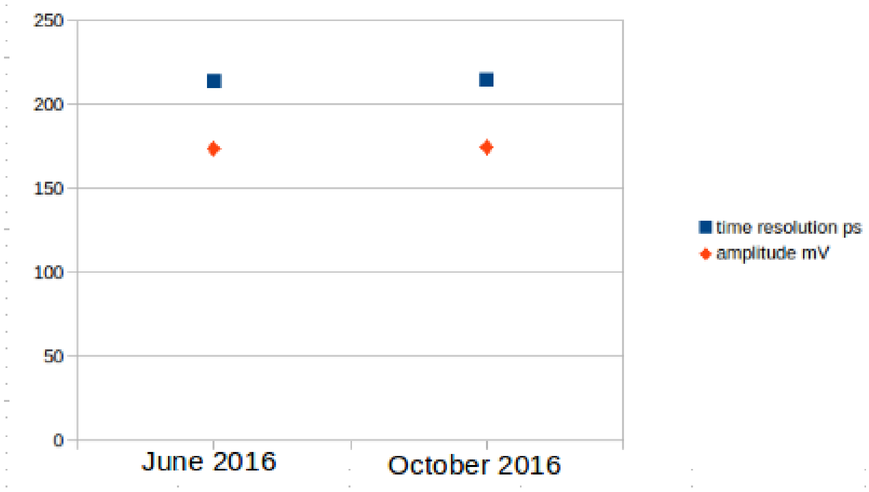

FIGURE 4.6: Time resolution and the amplitude of (Proto2+ EJ-204+ PMT19) 1400V in June and October.

The measurement showed that the grease does not change the signal amplitude or the time resolution after 4 months.

4.3.2 (Kuraray vs Mitsubishi Rayon) Fiber Bundle

(Kuraray vs Mitsubishi Rayon) Fiber Bundle Signal Amplitude. Figure (4.7) shows a comparison between the signal amplitude between (Kuraray vs Mitsubishi Rayon) Fiber Bundle (proto2 and proto5). The data in Figure (4.7) were all taken with fine mesh PMT19.

Proto5 has a less light transmission than proto2, it gives 65 mV in comparison to 174 mV for proto2 with factor 2.7 less at (1400V and scintillator EJ204). Mitsubishi fibers (proto5) has NA=0.5, Kuraray fibers (proto2) has NA=0.7, and that explains partially the low gain of proto5.

Proto2 vs Proto5 Time Resolution The data in Figure (4.8) were all taken with fine mesh PMT19. Proto5 has a worse time resolution than proto2, that partially could be attributed due to less signal amplitude. The best achieved time resolution of proto5 is $\sigma \sim 293$ ps (with scintillator EJ204 and PMT).

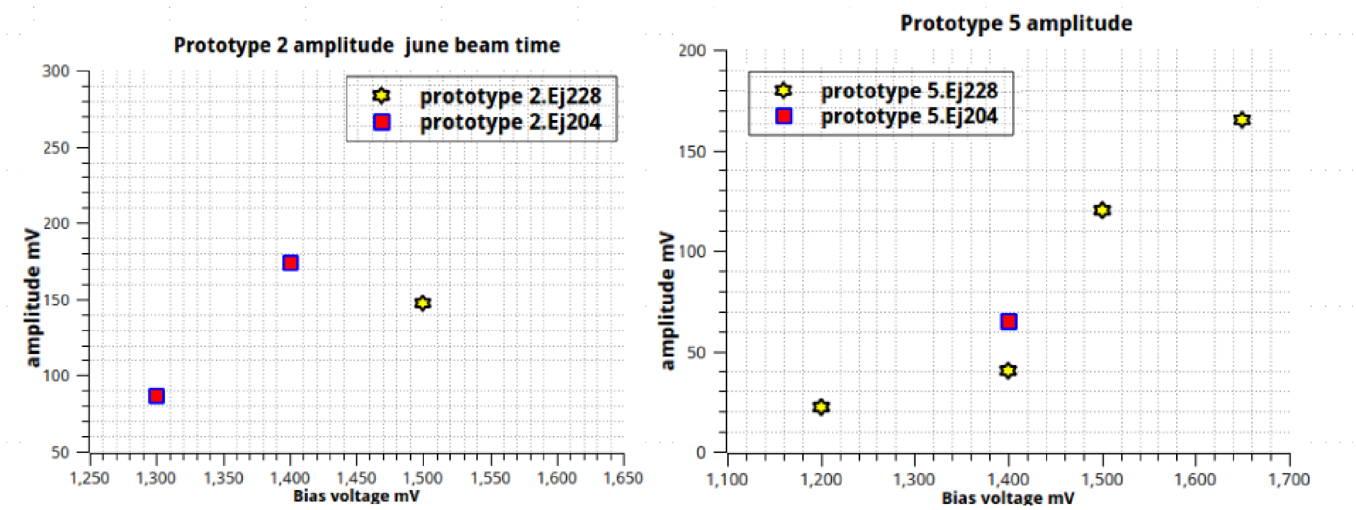

FIGURE 4.7: Signal amplitude of Proto2 vs proto5.

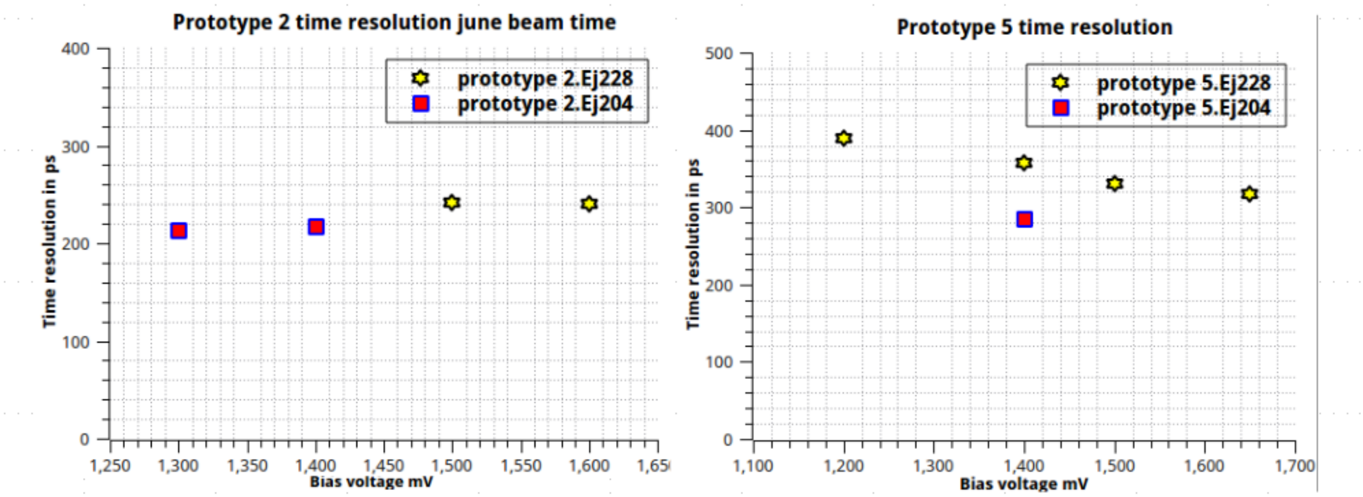

FIGURE 4.8: Time Resolution of Proto2 vs proto5.

4.3.3 Increasing the Dynamic Range

As the read output electronics of the FIT detector can not read more than 5V, and the and dynamic range should be able to read up to 500 particles so that we need to reach 10 mV per MIP.

(Proto 2 + EJ-204 + PMT 19 + Ortec pre-amp x10 amplification) this configuration was tested at a low bias voltage to decrease the gain in order to obtain a higher dynamic range, Figure (4.9) shows the signal amplitude and time resolution at a low bias voltage.

At low bias voltage (900-1000 V) we could get almost the same time resolution from June 2016 beam time. At a bias voltage of 1000 V, using an amplifier with magnification

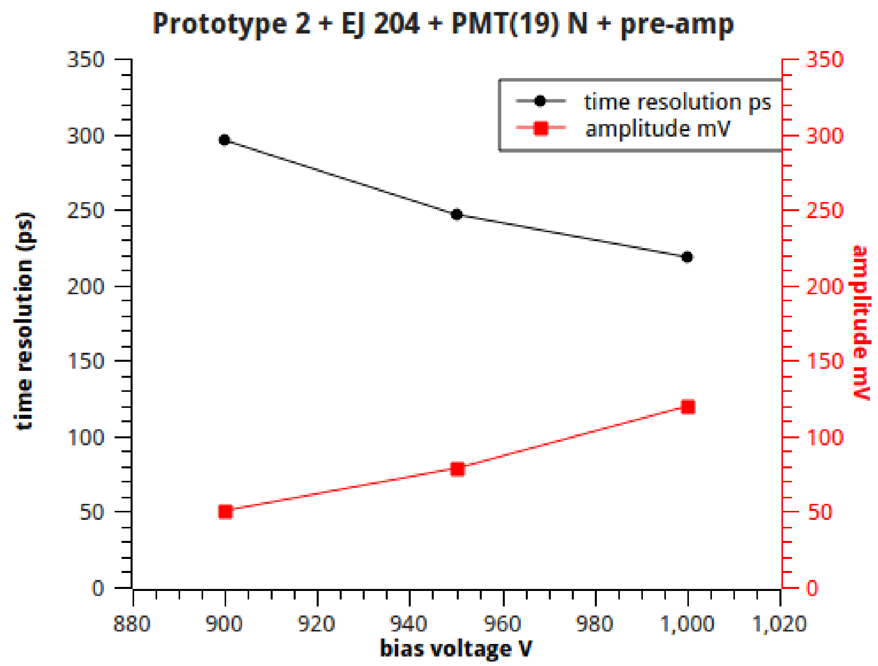

FIGURE 4.9: Signal amplitude and time resolution at low bias voltage.

factor x10 we reached a larger dynamic range than before 12 mV per MIP and also a good time resolution $\sigma \sim 220$ ps.

4.4 Summary

From all taken data during the beam times, we could conclude that: The scintillator of choice for V0+ is EJ-204, as it gives more light than EJ-232 and EJ-228, it also gives a better time resolution with all the tested fiber bundles except with Asahi round fibers they have a quite better time resolution with EJ-228.

Scintillator with one large side paint has better performance, however, stability over time needs to be tested due to the surface crack formation.

Round fibers give a definitely better time resolution and amplitude than square fiber. Kuraray and Asahi round fibers with 1 mm diameter give the best performance among the all tested fiber models, however, Kuraray still gives a slightly better performance when it is coupled to EJ-204.

Pyramid-shaped plastic light guide with factor 4 surface reduction does not deteriorate the time resolution. The FOT and conical light guide options were discarded due to the bad time resolution and low amplitude.

The poor time resolution and pulse amplitude discarded the SiPM and MCP-PMT solution for the V0+ detector. Fine-mesh (Hamamatsu) PMT seems to be a good option for V0+.

The best measured time resolution was the combination of (EJ-204 + Kuraray fiber + FM-PMT) $\sigma \sim 210$ ps. This combination gives the best performance of all the other combinations.

The dynamic range could be increased by applying low bias voltage ~ 1000 V to the Fine-mesh PMT, so we could go with signal amplitude down to 12 mV per MIP and time resolution $\sigma \sim 220$ ps.

.

Appendix A

TABLE A.1: The position efficiency across x-axis.

X-axis	Mean value (V)	Stander div σ	Local efficiency
-14	1.49	107.1	21±1.6
-12	2.03	127.7	28.7±2.1
-10	2.5	133.7	35±2.4
-8	2.87	158.8	40.55±2.7
-6	3.12	160.8	44.1±2.9
-4	3.27	156.3	46.2±2.9
-2	3.34	158.4	47.2±,2.9
0	3.44	156.5	48,6±3
2	3.35	157.5	46.2±3
4	3.27	161	40.2±3
6	2.98	161	40.2±3
8	2.6	148.8	36.7±3
10	2.38	134.8	33.6±2,6
12	1.94	129.6	27.4±2.2
14	1.32	100.5	18.6±1.6

TABLE A.2: The position effeciancy accross y.

X-axis	Mean value (V)	Stander div σ	Local efficiency
-14	1.46	106.5	20.6 $\pm$1,6
-12	1.85	125.8	26.1$\pm$2.1
-10	1.94	124.7	27.4$\pm$2.4
-8	2.46	133.4	34.7$\pm$2.7
-6	2.68	149.5	37.9$\pm$2,9
-4	2.76	155.6	39$\pm$2.9
-2	2.82	158.5	39$\pm$2.9
0	3.2	156	45.2$\pm$3
2	3.03	159.5	42.8$\pm$3
4	2.91	160.8	41.1$\pm$3
6	2.84	158	40.1$\pm$3
8	2.47	131.6	34.8$\pm$3
10	2.35	126.3	33.1$\pm$2.6
12	2.09	123.4	26,7$\pm$2.2
14	1.62	117.3	22.8$\pm$1.6

TABLE A.3: Testing the total light efficiency of FOT and light guide using LED

Type of measurement	Pulse height (V)	Stander div σ	Number of events
Reference	-4.5864	193.4	10 061
Light Guide	-3.3513	544.8	10 243
FOT	-2.0748	131.0	10 264

TABLE A.4: Testing the total light efficiency of FOT and light guide using Laser

Type of measurement	Pulse height (V)	Stander div σ	Number of events
Reference	-4.3531	220.1	1594
Light Guide	-3.6302	220.9	5763
FOT	-0.429	63.87	5555

TABLE A.5: Scan of the plastic light guide with Laser

Position	Mean value (V)	Local efficiency	Stander div σ
(-3,0)	-2.7466	0.664	191.0
(-2,0)	-3.2155	0.777	194.6
(-1,0)	-3.3262	0.804	196.7
(0,0)	-3.3773	0.816	198.2
(1,0)	-3.3531	0.811	199.7
(2,0)	-3.0706	0.742	189.7
(3,0)	-2.3864	0.577	168.3
(0,-3)	-2.6291	0.636	185.6
(0,-2)	-3.2279	0.780	199.0
(0,-1)	-3.3907	0.820	201.6
(0,1)	-3.4344	0.830	200.5
(0,2)	-3.2757	0.792	198.6
(0,3)	-2.4681	0.597	177.8
Reference	-	-4.1366	217.6

TABLE A.6: Scan of the FOT with Lase

Position	Mean value (V)	Local efficiency	Stander div σ
(-3,0)	-285.263	0.0696	55.560
(-2,0)	-347.48	0.0848	63.17
(-1,0)	-347.851	0.0849	62.582
(0,0)	-368.58	0.0900	64.57
(1,0)	-357.26	0.0872	63.97
(2,0)	-329.448	0.0804	60.284
(3,0)	-245.506	0.0599	51.618
Reference	-4096.05		218.9

TABLE A.7: The signal amplitude and current at different frequencies.

Frequency	Signal amplitude mV	Current μA
1 kHZ	9.5	1
10 kHZ	9.5	2
52 kHZ	9.6	4.5
102 kHZ	9.5	7.6
450 kHz	9.1	2.9
740 KHz	8.5	45
1 MHz	7.8	56
1.2 MHz	6.7	55
1.3 MHz	6	54

TABLE A.8: The signal amplitude and current at different frequencies.

Frequency kHz	Signal Amp mV at 54 V	Signal Amp mV at 55 V
1	18.5	32.9
20	18.6	32.8
50	18.5	32.6
100	18.2	32.2
300	17.4	30.6
500	16.5	29
700	15.8	24.3
800	15	21.3
900	14.7	19
1000	14.1	17.2
1100	13.7	15.7

TABLE A.9: The signal amplitude of PMT at different frequencies.

Frequency kHz	Signal Amp mV (at 1600 V)	Signal Amp mV (at 1800 V)
10	209	561
50	207	563
100	208	
150	207	563
250	207	
400	207	563
600	204	560
800	200	554
900	193	544
1,000	182	520
1,100	178	513
1,200	176	501
1,300	170	490

TABLE A.10: The tested component during June beam time

Scintillator (10x10x4 cm3)	Fiber(Ø =1mm)	Light guide (plastic)	Photodetector
EJ-204	Bicron (square)	pyramidal-shape	Fine mesh PMT 16 stages
EJ-228	Kuraray (round)	conical	Fine mesh PMT 19 stages
-	Asahi (round)	no light guide	MCP-PMT
-	-	-	SiPM Hamamatsu (6x6 mm^2
-	-	-	PMT (current V0)
-	-	-	SiPM Ketek (6x6 mm^2)

TABLE A.11: Definition of the Scintillators

Scintillator Model	Manufacturer	Abbreviation	Size
EJ-204	Eljen Technology	(10 x 10 x 4 cm3)	10x10x4 cm3
Ej 228	Eljen Technology	Ej 228	10x10x4 cm3

TABLE A.12: Definition of Light Concnetrator

Abbreviation	Material	Shape	Length(mm)	Ø in(mm)	Ø out(mm)	Manufactured
FOT	fiber	-	50	30	9	OSJC
LGV1a	plastic	conical	50	30	9	Vienna
LGV1b	plastic	conical	50	30	9	Vienna
LGV2	plastic	conical	50	22,5	7	Vienna
LGV3	plastic	conical	60	30	9	Vienna
LGV4a	plastic	conical	50	30	7	Vienna
LGV4b	plastic	conical	50	30	7	Vienna
LGM1	plastic	pyramid	21	22	11	Mexico
LGM2	plastic	pyramid	10	11	6	Mexico
LGM3	plastic	pyramid	30	21	6	Mexico
LGM4	plastic	pyramid	20	20	10	Mexico

TABLE A.13: Definition of Photo Sensor

Abbreviation	Manufacturer	Model
PMT 19	Hamamatsu	H8409-70
PMT 16	Hamamatsu	H6153-70
PMT 15	Hamamatsu	H6152-01B
SiPM (6x6mm2)	Hamamatsu	S13360-3050PE
MCP-PMT	-	-

TABLE A.14: Definition of the Fiber Bundle

Abbreviation	Shape	Manufacturer	Pitch	Fiber	Cladding	NA	Model
Proto1	square	bicron	5 mm	400	double	-	-
Proto2	round	kuraray	5 mm	400	double	0.7	Clear-PSM
Proto3	round	Asahi	5 mm	400	single	0.6	SB-1000
Proto4	square	bicron	7 mm	196	double	-	-
Proto5	round	Mitubishi	5 mm	400	single	0.5	SK-40

Bibliography

[1] On behalf of the ALICE collaboration E. Garcia-Solis. “The Fast Interaction Trigger Upgrade for ALICE”. In: *38th International Conference on High Energy Physics 3-10 August 2016 Chicago, USA* 267 ().

[2] ALICE collaboration. *ALICE matter*. http://alicematters.web.cern.ch/?q=ALICEoverview.

[3] C Fabjan and J Schukraft. “The story of ALICE: Building the dedicated heavy ion detector at LHC”. In: *arXiv preprint arXiv:1101.1257* (2011).

[4] Edmundo Garcia-Solis, ALICE Collaboration, et al. “Perspectives of the ALICE Experiment and Detector Upgrade”. In: *Nuclear and Particle Physics Proceedings* 267 (2015), pp. 382–391.

[5] Lyndon R Evans. *The Large Hadron Collider: a marvel of technology*. EPFL Press, 2009.

[6] Xabier Cid Vidal and Ramon Cid Manzano. *Luminosity*. https://www.lhc-closer.es/taking_a_closer_look_at_lhc/0.luminosity. 2015.

[7] B Abelev et al. “Technical design report for the upgrade of the ALICE Inner Tracking System”. In: *Journal of Physics G: Nuclear and Particle Physics* 41.8 (2014), p. 087002.

[8] ALICE collaboration et al. “Upgrade of the ALICE Time Projection Chamber”. In: *CERN-LHCC-2013-020* (2013).

[9] ALICE collaboration et al. “Addendum of the letter of intent for the upgrade of the ALICE experiment: the Muon forward tracker”. In: *CERN-LHCC-2013-014* (2013).

[10] Jacobus Willem Van Hoorne. “The upgrade of the ALICE Inner Tracking System-Status of the R&D; on monolithic silicon pixel sensors”. In: *PoS* (2014), p. 125.

[11] Wladyslaw Henryk Trzaska, ALICE Collaboration, et al. "New Fast Interaction Trigger for ALICE". In: *Nuclear Instruments and Methods in Physics Research Section A: Accelerators, Spectrometers, Detectors and Associated Equipment* (2016).

[12] M Bondila et al. "ALICE T0 detector". In: *IEEE transactions on nuclear science* 52.5 (2005), pp. 1705–1711.

[13] ALICE Collaboration, E Abbas, et al. "Performance of the ALICE VZERO system. JINST 8". In: *P10016* (2013), pp. 1748–0221.

[14] W.H.Trzaska. *FIT Collaboration Meeting*. https://indico.cern.ch/event/367850/. [Online; accessed 21-January-2015]. 2015.

[15] CERN. *SBA secondry beam and area*. http://sba.web.cern.ch/sba/BeamsAndAreas/East/East.htm. 2013.

[16] L.Grabski. *FIT Collaboration Meeting*. https://indico.cern.ch/event/461198/. [Online; accessed 12-Nov-2015]. 2015.

[17] KETEK GmbH. *KETEK Silicon Photomultipliers SiPM*. http://www.ketek.net/products/sipm/.

[18] wikipedia. *Winston cone*. https://en.wikipedia.org/wiki/Winston_cone. 2016.

[19] Eljen. *Plastic-scintillators*. http://www.eljentechnology.com/products/plastic-scintillators.

[20] OJSC. *Fiber optic tapers*. http://www.opticlida.by/en/voloconno-opticheskie_fokony/.

[21] Claus Grupen and Irène Buvat. *Handbook of particle detection and imaging*. Springer Science & Business Media, 2011.

[22] Brian F Aull et al. "Geiger-mode avalanche photodiodes for three-dimensional imaging". In: *Lincoln Laboratory Journal* 13.2 (2002), pp. 335–349.

[23] Hamamatsu Photonics. "Opto-semiconductor handbook"". In: (2009).

[24] Advatech.UK Ltd. *SiPM Preamplifiers*. http://www.advatech-uk.co.uk/preamps_sipm.html. [Online; accessed 30-Nov-2016].

[25] Paolo W Cattaneo et al. "Development of high precision timing counter based on plastic scintillator with SiPM readout". In: *IEEE Transactions on Nuclear Science* 61.5 (2014), pp. 2657–2666.

[26] S-O Flyckt. *Photomultiplier tubes: principles and applications*. Photonis, 2002.

[27] KK Hamamatsu Photonics. "PHOTOMULTIPLIER TUBES, Basics and Applications". In: *Hamamatsu Photonics K.K.* (2006).

[28] Hamamats. *Hamamatsu Photonics K.K.* http://www.hamamatsu.com/eu/en/community/optical_sensors/articles/intro_to_uPMT/index.html.

[29] Albert Einstein. "The photoelectric effect". In: *Ann. Phys* 17.132 (1905), p. 4.

[30] wikipedia. *Microchannel plate detector*. https://en.wikipedia.org/wiki/Microchannel_plate_detector.

[31] PHOTONIS. *PLANACON-8x8-datasheet*. https://https://www.photonis.com/uploads/datasheet/pd/PLANACON-8x8-datasheet.pdf. 2013.

[32] Stergios J Papadakis. *High gain photo and electron multipliers and methods of manufacture thereof*. US Patent 9,102,524. 2015.

[33] CAEN. *Desktop Waveform Digitizer*. http://www.caen.it/jsp/Template2/CaenProd.jsp?parent=14&idmod=651.

[34] CERN. *ROOT Data Analysis Framework*. https://root.cern.ch/.